Paweł Rejmak

Self Report

The structural and spectroscopic properties of aluminosilicate materials determined with computational methods.

Institute of Physics, Polish Academy of Sciences

Table of Contents

1 Personal Data

Name and Surname

Paweł Rejmak

Education

2008 Doctoral degree in chemistry (with honors).
Thesis title: *"Investigation of Cu(I) Sites in FAU and MFI Zeolites and their Interactions with Small Molecules: Quantum Chemical and Hybrid QM/MM Studies"*, supervisor: prof. Ewa Brocławik.

2003–2008 PhD studies at Institute of Catalysis and Surface Chemistry PAS, Kraków, Poland.

2003 Graduated in chemistry, Department of Theoretical Chemistry, supervisor: prof. Krzysztof Woliński.

1998-2003 Graduate studies at Faculty of Chemistry, Maria Curie-Skłodowska University, Lublin, Poland, chemistry degree course.

Employment history

11.2016–until now Assistant professor at Institute of Physics PAS, Laboratory of X-Ray and Electron Microscopy Research, Group of X-ray Spectroscopy and Microanalysis (SL-1.2).

11.2013–09.2016 Assistant professor at Institute of Physics PAS, Laboratory of X-Ray and Electron Microscopy Research, Group of X-ray Spectroscopy and Microanalysis (SL-1.2), employment within EAgLE project.

06.2010–10.2013 Postdoc position in Donostia International Physics Center, Donostia-San Sebastián, Hiszpania.

2009–2010 Technician at Institute of Catalysis and Surface Chemistry PAS (since 06.2010 on unpaid leave, due to departure to postdoc position).

Bibliometrics

ReasercherID	S-5837-2016
ORCID	0000-0002-0535-2107
The number of publications indexed in Web of Science	28
Citations	437 (407 without self-citations)
Hirsch Index	11

All bibliometrics according to Web of Science portal, the status at 30.08.2022.

2 The description of scientific achievement, as specified in art. 219 para 1 point 2 of the Act

Cycle of topically linked scientific papers

[**H1**] **P. Rejmak**, J. S. Dolado, M. J. Stott, A. Ayuela, "^{29}Si NMR in Cement: A Theoretical Study on Calcium Silicate Hydrates", *Journal of Physical Chemistry C* **2012**, *116*, 9755–9761.
IF_{2021} = 4.177, citations = 76, corresponding author.

[**H2**] **P. Rejmak**, J. S. Dolado, M. J. Stott, A. Ayuela, "^{29}Si Chemical Shift Anisotropies in Hydrated Calcium Silicates: A Computational Study", *Journal of Physical Chemistry C* **2013**, *117*, 8374–8380.
IF_{2021} = 4.177, citations = 11, corresponding author.

[**H3**] A. Cuesta, A. G. De la Torre, E. R. Losilla, V. K. Peterson, **P. Rejmak**, A. Ayuela, C. Frontera, M. A. G. Aranda, "Structure, Atomistic Simulations, and Phase Transition of Stoichiometric Yeelimite", *Chemistry of Materials* **2013**, *25*, 1680–1687.
IF_{2021} = 10.508, citations = 100.

[**H4**] A. Cuesta, **P. Rejmak**, A. Ayuela, A. G. De la Torre, I. Santacruz, L. F. Carrasco, C. Popescu, M. A. G. Aranda, "Experimental and theoretical high pressure study of calcium hydroxyaluminate phases", *Cement and Concrete Research* **2017**, *97*, 1–10.
IF_{2021} = 11.958, citations = 8.

[**H5**] **P. Rejmak**, "Structural, Optical, and Magnetic Properties of Ultramarine Pigments: A DFT Insight", *The Journal of Physical Chemistry C* **2018**, *122*, 29338–29349.
IF_{2021} = 4.177, citations = 6, corresponding author.

[**H6**] **P. Rejmak**, J. S. Dolado, M. A. G. Aranda, A. Ayuela, "First-Principles Calculations on Polymorphs of Dicalcium Silicate — Belite, a Main Component of Portland Cement", *The Journal of Physical Chemistry C* **2019**, *123*, 6768–6777.
IF_{2021} = 4.177, citations = 9.

[**H7**] **P. Rejmak**, J. Datka, E. Broclawik, "Identity of two types of strong Brønsted acid sites in mazzite revealed by CO probe: IR study and periodic DFT modeling", *International Journal of Quantum Chemistry* **2019**, *119*, e25873.
IF_{2021} = 2.437, citations = 2.

[**H8**] **P. Rejmak**, "Computational refinement of the puzzling red tetrasulfur chromophore in ultramarine pigments", *Physical Chemistry Chemical Physics* **2020**, *22*, 22684–22698.
IF_{2021} = 3.945, citations = 3, corresponding author.

2.1 Introduction

Silicates, aluminates, and aluminosilicates, namely salts containing oxoanions of silicon and/or aluminum, constitute an unusually rich and heterogeneous group of inorganic solids. They are the main ingredient of the crust of Earth and other rocky planets, as well as they are employed on a massive scale as ceramics, building materials, adsorbents, catalysts, or pigments. Silicon atom preferably binds to four O atoms, the positions of the latter determine the corners of coordination tetrahedron. Due to similar chemical properties, Al atoms frequently substitute Si positions in these polyhedra within the wide range of stoichiometry. The crystallographic structures of aluminosilicate frameworks built of (SiO_4) and (AlO_4) units are usually solved assuming the presence of generalized tetrahedrally coordinated atoms, referred to as 'T atoms', whereas the exact distribution of Si and Al atoms throughout the crystallographic positions of T atoms remains unknown. Moreover, Al in connectivity to O willingly adopts octahedral coordination, only exceptionally found for Si.[1]

Many aluminosilicates are only partially ordered systems, hence the possibilities to characterize them structurally with diffraction methods are limited. For instance, the invoked issue of determining Si and Al atoms distribution among the framework T positions, which can be substantial *e.g.* for the catalytic properties of aluminosilicates. The substitution of Si^{4+} by Al^{3+} in the starting silicate lattice demands the charge compensation by additional cations (metallic or H^+) in addition to TO_x framework. These extraframework cations in aluminosilicates are frequently too poorly ordered or have a too low concentration (at low Al loadings) to give a clear diffraction pattern. Also, the geometries of molecules, adsorbed or occluded in porous aluminosilicates, are usually not well resolved by crystallographic methods, due to an aperiodic arrangement and mobility of the aforementioned molecules, Last but not least, certain commonly applied aluminosilicates, like glasses and hydrated cements, are amorphous solids. The spectroscopic methods are a valuable source of information on disordered materials, however, data obtained in this way are often ambigous, and their interpretation reported in the literature is frequently arbitrary.

In a view of described difficulties, the computational methods of theoretical chemistry and solid state physics, especially these treating electronic structure explicitly, offer the valuable support for the experimental studies on aluminosilicates. The computational methods allow determining equilibrium geometries, vibrational frequencies, elastic properties, electronic structure and stemming from the latter spectroscopic properties (*e.g.* nuclear magnetic shielding). The computational approaches have many limitations, originating from both the approximated solutions of electronic structure, and the simplifications of the applied structural models of aluminosilicates, nevertheless they often allow interpreting the experimental data reasonably, as well as obtaining the information not available directly or in a simple way from an experiment.

The scientific achievement of mine, being an important contribution to the science of materials based on Si–O and Al–O bonds, is the determination of structural and spectroscopic properties of selected applied materials based on Si–O and Al–O linkages, namely cements, catalytic zeolites, and ultramarine pigments, with atomistic simulations. The main research method was periodic simulations employing the Density Functional Theory (DFT) level with gradient exchange-correlation functional. The above approach is currently one of the most popular methods of determining the electronic structure in solid state physics and chemistry, compromising the quality of results and computational cost. In some cases, depending on the adopted model and scientific problem, I employed also more approxima-

[1] SiO_6 octahedra are found in stishovite, one of SiO_2 polymorphs, and in thaumasite $Ca_3Si(OH)_6(CO_3)(SO_4)\cdot 12H_2O$.

ted or more advanced methods. Therefore, to optimize models of cements with large unit cells I applied approximated methods of molecular mechanics (MM), whereas for determination of electronic excitation energies in cluster models hosting polysulfur chromophores I employed DFT calculations with hybrid functionals.

I started the discussed investigations, which results contribute to the scientific achievement, during my postdoctoral fellowship in Donostia International Physics Center in Donostia–San Sebastián, Spain, in the course of 2010-2013, where I performed simulations of nuclear magnetic resonance (NMR) spectra for various models of hydrated cements [**H1**, **H2**], as well as investigated structure and compressibility of crystalline aluminates being components of high alumina cements [**H3**]. After a few years break from this research field, due to undertaking new research activities (DFT calculations for the bioactive Cu(II) complexes) within the EAgLE project, implemented in the Institute of Physics PAS, I reverted to computational studies on cements in collaboration with theoretical and experimental groups from Spain, which resulted in two published papers, the first dealing again with the compressibility of crystalline aluminates [**H4**], and the second devoted to the polymorphs of calcium orthosilicate, the main component of dry Portland cement [**H6**]. The independent field of my research devoted to chemistry and physics of aluminosilicates, which I began upon the accomplishment of EAgLE project, are the computational studies on ultramarine pigments, *i.e.* nanoporous aluminosilicates hosting polysulfur chromophores. I studied the structural and vibrational properties of ultramarines with periodic DFT calculations, whereas for optical excitations and g tensor for electron paramagnetic resonance I applied DFT calculations for cluster models. I presented the obtained results in two one-author publications [**H5**, **H8**]. The third group of materials studied by me, apart from the cements and ultramarines, are zeolites, namely nanoporous, crystalline aluminosilicates with ion exchange abilities, widely applied in adsorption and catalysis. In the current scientific achievement I included one study, performed in collaboration with researchers from Jerzy Haber Institute of Catalysis and Surface Chemistry PAS, Kraków, concerning the characterization of Brønsted type acid centers in mazzite type zeolite [**H7**]. In all multi-authored research papers, I was the main author of their computational parts.

2.2 The detailed description of scientific achievement

2.2.1 The computational spectroscopy of ^{29}Si nuclear magnetic resonance for hydrated Portland cements [H1, H2]

The principal component of hydrated Portland cement, responsible for its mechanical properties, is the amorphous or poorly crystalline hydrated calcium silicate, known as C–S–H gel. The last acronym employs commonly accepted in cement science the shorthand notation for stoichiometry, expressed by the content of given oxides, *e.g.* C=CaO, S=SiO_2, A=Al_2O_3 and H=H_2O. The replacement of numerical indicators by hyphens refers to the variable stoichiometry of C–S–H gel, which approximately amounts to $(CaO)_{1.7}(SiO_2)(H_2O)_{(1.2-1.8)}$ (or $C_{1.7}SH_{(1.2-1.8)}$ in described convention). The low ordering of C–S–H gel prohibits the exact solution of its structure, however, the combined efforts of diffraction methods, electron microscopy, NMR spectroscopy, and chromatography showed that C–S–H gel structure consists of finite length silicate anions, each containing $(3m\text{-}1)$ Si atoms ($m \geq 1$), forming parallel layers, separated by the layers of Ca^{2+} cations and water.

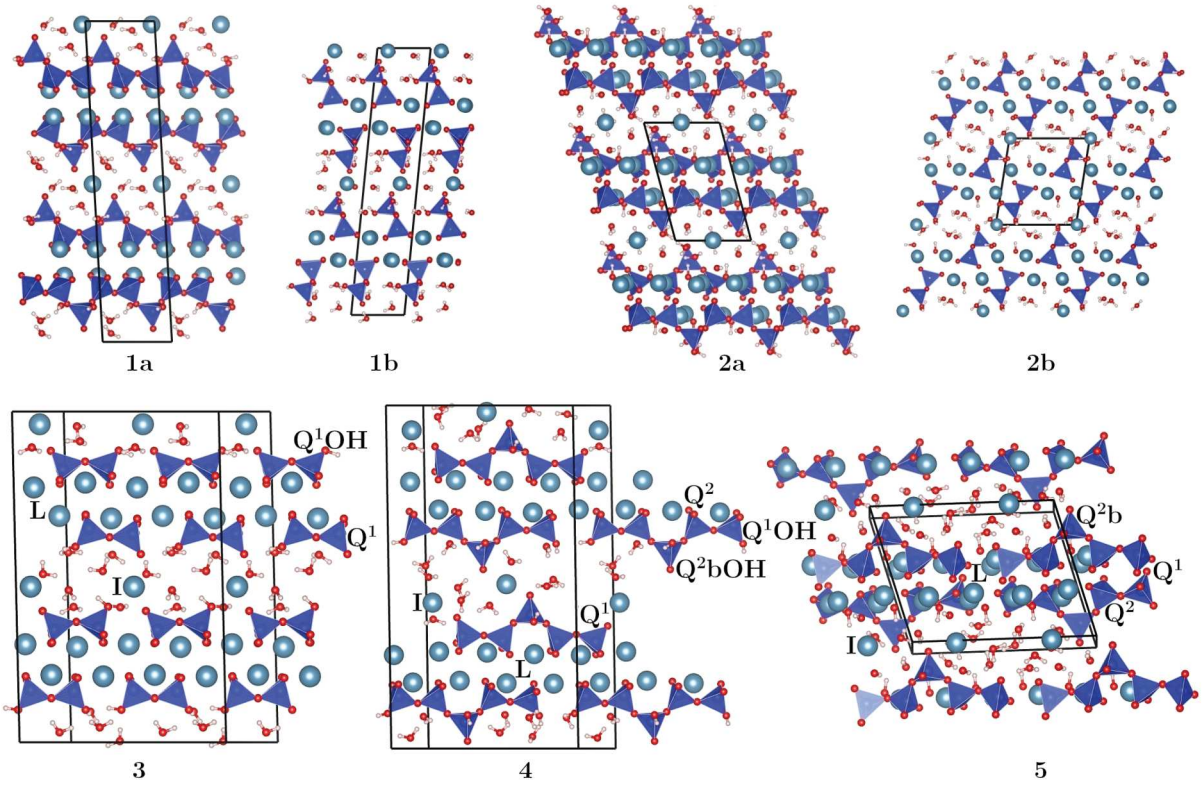

Figure 1: *The crystal structures of hydrated calcium silicates and derived models of C–S–H gel: (1) tobermorite 14 Å (a) [100] and (b) [010] projections, (2) jennite, (a) [100] and (b) [010] projections, (3) the dimeric model of C–S–H derived from tobermorite structure, (4) pentameric model of C–S–H gel derived from tobermorite structure, (5) pentameric model of C–S–H gel derived from jennite. For C–S–H gel models the initial unit cells of minerals were doubled along b direction. Q^1/Q^2 denote tetrahedra coordinated with one or two other tetrahedra, respectively, 'b' denotes tetrahedron in bridging position, 'OH' denotes the presence of protonated O atom. I/L denote Ca^{2+} in the interlayer/layer positions, respectively. The elements coloring: Ca–light-blue, Si–dark-blue, O–red, H–white.*

Various C–S–H gel models have been proposed, the common feature of them is representing C–S–H gel as the defected mineral of 14 Å tobermorite type [2] or jennite (JEN) type.[3]

The silicate chains within the ideal crystal of JEN or TOB14 are infinitely long, with two non-equivalent types of SiO_4 tetrahedra: two of three tetrahedra share their edges with CaO_6 octahedra, whereas every third tetrahedron occupies bridging position, in which it shares only oxygen corners with Ca coordination polyhedra, see Fig. 1. The removal of each or every second bridging tetrahedron generates structures built of silicate dimers or pentamers, respectively, which is consistent with experimental data for hydrated cements. The proposed structural models of C–S–H gel derived from the aforementioned crystalline minerals gave the results roughly consistent with the available experimental data, however, it was still unclear whether any type of model is closer to reality. The aim of my studies, performed at DIPC in the group of prof. Andres Ayuela, was to predict ^{29}Si NMR spectra employing electronic structure methods for various models of C–S–H gel, derived from both

[2] The tobermorite group contains several species of minerals, differing mainly by the water content and associated with this the spacing between silicate layers, hence the names 14/11/9 Å tobermorite.

[3] I. G. Richardson, *Cem. Concr. Res.* **2008**, *38*, 137–158.

JEN and TOB14, in order to find out, which type of model gives better agreement with the experiment.

I constructed the models of C–S–H gel using the experimental structures of JEN and TOB14 as starting points.[4] The main differences between JEN and TOB14 are (i) the presence of the layers of hydroxyl anions coordinating the Ca^{2+} layers in JEN, causing almost twice higher C:S ratio than in TOB14, (ii) the protonation of bridging tetrahedra in TOB14. The construction of an oligomeric model from crystalline JEN is achieved by the removal of electroneutral (SiO_2) unit, whereas in TOB14 the removal of each positively charged $[SiO(OH)]^+$ fragment requests for the charge compensation by additional cations: Ca^{2+} (one per two removed bridging tetrahedra), $Ca(OH)^+$ or H^+. The initial JEN and TOB14 unit cells were doubled along the direction of silicate chains, so that such supercell could host (upon the removal of every second bridging tetrahedron) silicate pentamer. For my purposes, I constructed in total 14 models of C–S–H gel containing silicate dimers and pentamers (9 derived from TOB14 and 5 from JEN), differing by the amount and distribution of charge compensating Ca^{2+}, $Ca(OH)^+$ and H^+ cations. Higher silicate ($3m$-1)-mers were not considered, because (i) such oligomers are present in small amounts only in well-aged cement pastes, (ii) their computational treatment would demand supercells too large for DFT.

By definition, the periodic model cannot strictly represent the amorphous solid. The common approach in studying the aperiodic bulks is the employment of large supercells, in order to keep the periodic images of corresponding atoms as far apart as possible. The use of large structural models usually enforces their treatment with approximate computational methods, such as MM or tight binding models. In my work, I needed to compute the spectroscopic properties with more computationally expensive electronic structure methods, hence the restriction of the model's size (unit cell volume and the number of electrons) was necessary. Eventually, I decided to perform DFT calculations for the series of periodic models with the modest size of a unit cell, and to draw conclusions for C–S–H gel upon averaging the results within a certain category of models.

Due to still large size of employed periodic models (for TOB14 models, the supercells contained over 200 atoms and had volumes over 1100 $Å^3$) I optimized geometry at MM level using GULP programme, [5] with polarizable interatomic potential functions.[6] For the structures optimized in that way I performed periodic electronic structure calculations at DFT level using QUANTUM ESPRESSO package,[7] which employs plane-wave (PW) basis sets for the description of valence region electrons and offers several ways to treat the core region electrons, including the Projector Augmented Waves approach (PAW),[8] establishing a one-to-one correspondence between the all-electron wavefunctions and their monotonic tails in the valence region. In my studies I employed Perdew-Burke-Ernzerhof (PBE)[9], gradient exchange-correlation functional, the norm-conserving Troullier-Martin[10] pseudopotentials, and the cutoff energy for PW of 80 Ry. The Brillouin zone in TOB14 models was sampled with 2×1×1 mesh (namely 2 points in the direction correspon-

[4] JEN structure: E. Bonaccorsi, S. Merlino, H.F.W. Taylor, *Cem. Concr. Res.* **2004**, *34*, 1481–1488; TOB14 structure: E. Bonaccorsi,S. Merlino, A. R. Kampf, *J. Am. Ceram. Soc.* **2005**, *88*, 505-512.

[5] J. D. Gale, *J. Chem. Soc., Faraday Trans.* **1997**, *93*, 629–637.

[6] The employed parametrization was taken from the following papers – Si–O: M. J. Sanders, M. Leslie, C. R. A. Catlow, *J. Chem. Soc., Chem. Commun.* **1984**, 1271–1273; Ca–O: G. V. Lewis, C. R.A. Catlow, *J. Phys. C: Solid State Phys.* **1985**, 18, 1149–1161; H–O: Z. Du, N. H. de Leeuw, *Surf. Sci.* **2004**, *554*, 193–210.

[7] P. Giannozzi *et al.*, *J. Phys.: Condens. Matter.* **2009**, *21*, 395502.

[8] P. Blöchl, *Phys. Rev. B* **1994**, *50*, 17953-17979.

[9] J. P. Perdew, K. Burke, M. Ernzerhof, *Phys. Rev. Lett.* **1996**, *77*, 3865.

[10] N. Troullier, J. L. Martins, *Phys. Rev. B* **1991**, *43*, 1993-2006.

ding to the shortest lattice constant in real space, being roughly 7 Å), and simply with Γ point in JEN models. To compute the magnetic shielding tensor of ^{29}Si nuclei I used gauge independent PAW (GIPAW) method[11], which enables the determination of periodic systems response to the external magnetic field.

Magic angle spinning NMR is one of the principal methods employed for the characterization of cements, notably the amorphous phases.[12] In ^{29}Si NMR the position of Si in $(SiO)_4$ tetrahedron linked via O corners to n other tetrahedra is commonly denoted as Q^n, where n adopts values from 0 (orthosilicates) to 4 (SiO_2). For ^{29}Si the isotropic chemical shift δ_{iso} decreases (*i.e.* shielding increases) with the increase in the condensation of silica tetrahedra, however, its particular value depends also on many other factors. Therefore, the observed ranges of δ_{iso} for $Q^n/Q^{(n+1)}$ partially overlap. In C–S–H gel one can see almost exclusively the signals from ^{29}Si in Q^1 and Q^2 sites, (the typical signals are around -80 and -85 ppm, respectively), which confirms the oligomeric structure of discussed solid.

The GIPAW values of isotropic shielding constants (σ_{iso}) for inequivalent of ^{29}Si nuclei show quite large dispersion, and their ranges partially overlap, as show in Fig. 2, however, they obey the general trend $Q^2 > Q^2b \approx Q^2bOH > Q^1 > Q^1OH$, see Fig. 1 for notation. The dispersion of ^{29}Si σ_{iso} values for nuclei in Q^2 position is smaller and less model dependent than in the case of Q^1 and Q^2b. The shielding of Q^1 sites is generally stronger in TOB models than in JEN ones, which can be explained by the presence of additional Ca^{2+} bridging Q^1 tetrahedra in the adjacent oligomers within TOB models. I calculated ^{29}Si δ_{iso} using the values of GIPAW σ_{iso} for the additional references (α–quartz and β–Ca_2SiO_4) and subsequently used them to plot spectra, which can be directly compared with experimental ones. Three such spectra are shown in Fig. 2, respectively for the models of C–S–H gel (i) TOB derived, with high Ca loading (Ca–TOB), (ii) TOB derived with low Ca loading/ charge compensation based on the protonation of terminal tetrahedra (H–TOB), (iii) JEN derived. For each spectrum I used data from one dimeric and three pentameric models. Dotted curves were obtained by summation of Gaussian functions centered around separate values of δ_{iso} for each ^{29}Si nuclei, whereas solid curves by the summation of Gaussians centered at mean values of δ_{iso} for each five different types of Q^n within a given model. The purpose of the latter averaging was to approximate roughly the averaging of observed signals due to the dynamical effects (lattice oscillations and the motions of interlayer H_2O molecules), absent in the considered static model. Among the obtained spectra, the best agreement with experiments was found for Ca–TOB models, reproducing the spectrum shape with two main signals, less shielded stemming mainly from terminal Q^1 and bridging Q^2b sites, and more shielded, mainly coming from Q^2 sites. The spectrum of H–TOB models has an additional intensive peak due to protonated terminal Q^1OH tetrahedra, shifted toward the higher values of δ_{iso}, not observed for hydrated cements. Finally, the spectrum of JEN models features large dispersion of δ_{iso} values, resulting in a multipeak spectrum, in qualitative disagreement with experimental data.

None of the tested models fully reproduced the experimental mass densities and stoichiometry of C–S–H gel, however, considering that (i) the density of C–S–H gel strongly depends on the amount of incorporated water and its packing (inside the structure or at the surface of gel grains),[13] and (ii) the considerable amount of Ca in hydrated cements

[11] C. J. Pickard, F. Mauri, *Phys. Rev. B* **2001**, *63*, 245101.
[12] B. Walkley, J. L. Provis, *Mater. Today Adv.* **2019**, *1*, 100007.
[13] J. S. Dolado, M. Griebel, J. Hamaekers, F. Heber, *J. Mater. Chem.* **2011**, *21*, 4445-4449.

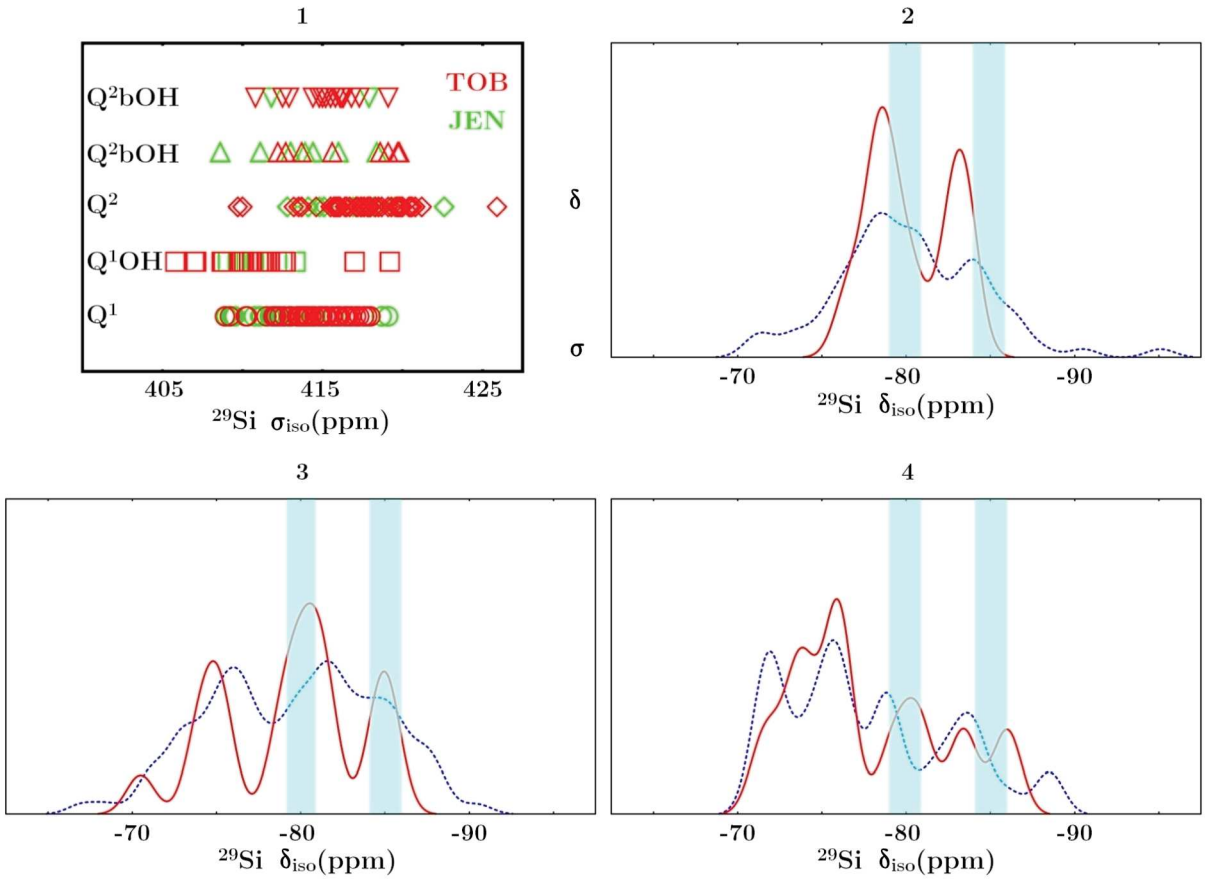

Figure 2: *The GIPAW results for C–S—H gel models: (1) the dispersion of isotropic shieldings (σ_{iso}) for the different types of Q^n, and the simulated ^{29}Si NMR spectra for C–S–H gel models of the following types: (2) TOB model, the unit cell charge compensation with additional Ca^{2+} ions, (3) TOB model, the unit cell charge compensation with additional H^+ ions, (4) JEN model. The shaded area indicates the typical range of experimental ^{29}Si isotropic chemical shieldings (δ_{iso}) in C–S–H gel. Dotted curves were obtained by the summation of Gaussian peaks centered around the individual values of δ_{iso} for each Si atom, whereas solid curves by the summation of Gaussian peaks centered around mean values of δ_{iso} for each of possible five types of Q^n within a given model.*

is present as $Ca(OH)_2$ intrusions,[14] Ca–TOB models of gel again are the closest to the experimental data.

The subsequent studies, resulting in the scientific paper [**H2**], focused the more detailed analysis of the components of σ tensor and employing the information contained in them for the structural characterization of C–S–H gel. This study was inspired by the experimental work by Skibsted and coworkers, who noticed, that ^{29}Si chemical shift anisotropy (CSA) enabled distinguishing of different Q^n, even if they have very similar values of σ_{iso}.[15]

The main results are shown in Fig. 3. Indexing by z, x, y the components of δ tensor with subsequently decreasing absolute values of deviation from the mean value of δ_{iso} one can define CSA as $(\delta_{iso} - \delta_{zz})$, and CSA asymmetry η as $(\delta_{xx} - \delta_{yy})$/CSA. Almost all ^{29}Si nuclei in Q^1 positions show, as the only ones, the negative values of CSA. All types

[14] J. J. Thomas, J. J. Chen, H. M. Jennings, *Chem. Mater.* **2003**, *15*, 3813-3817.
[15] M. R. Hansen, H. J. Jakobsen, J. Skibsted, *Inorg. Chem.* **2003**, *42*, 2368-2377.

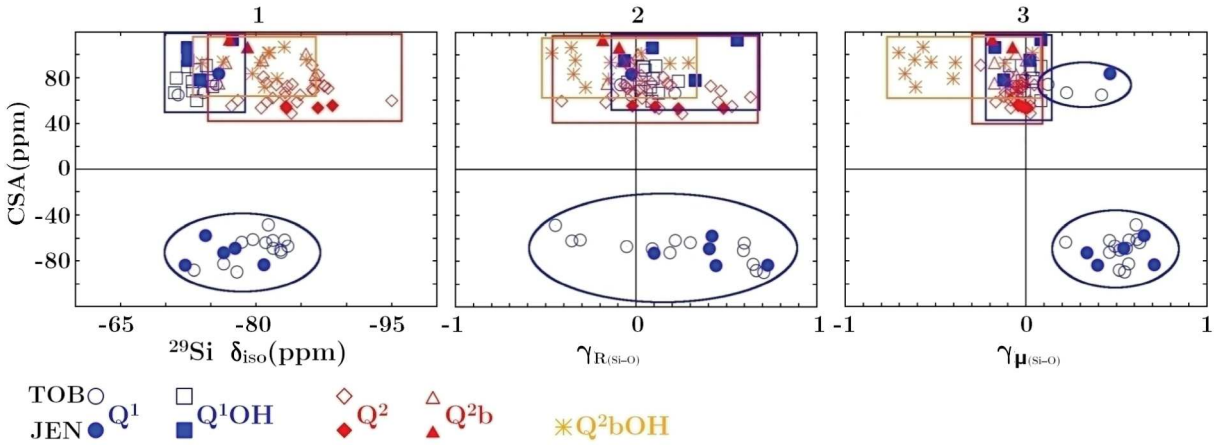

Figure 3: *The chemical shift anisotropy (CSA) of ^{29}Si nuclei obtained from GIPAW calculations for the models C–S–H plotted* vs. *(1) the isotropic chemical shift σ_{iso}, (2) the skewness (asymmetry measure) of the distribution of Si–O bond lengths in silica tetrahedra $\gamma_{R_{Si-O}}$, and (3) the skewness of the distribution of Si–O dipole moments $\gamma_{\mu_{Si-O}}$.*

of Q^2 sites, as well as Q^1OH, have positive CSA. Moreover, Q^2bOH reveals significantly smaller η (below 0.6) in comparison to the other Q^n. The differences in CSA of various Q^n sites are usually discussed in terms of different numbers of short and long Si–O bonds in tetrahedra (short bonds are these with unsaturated O atoms, terminating tetrahedron, long ones are with O atoms in a common corner of two tetrahedra). As a measure of the asymmetry in bond lengths distribution, I adopted skewness (γ, standardized third moment)[16] and plotted CSA *vs.* γ. Q^2, Q^2b and Q^1OH tetrahedra (with two short and two long bonds) exhibit γ values close to 0, whereas Q^1 (three short bonds and one long) and Q^2bOH (one short and three long bonds) usually reveal γ visibly lesser or greater than 0, respectively. The differences between various types of tetrahedra are even more evident when instead of bond lengths I applied bond dipole moments, defined as the product of bond length and the difference of atomic Löwdin charges calculated for Si and O.[17]

The obtained theoretical results showed that the analysis of δ tensor components enables speciation of different Q^n sites, as well as detecting the presence of O—H bondings in SiO_4 tetrahedra. Unfortunately, the measurement of CSA for the amorphous solids is much harder than for crystals (where the principal components of δ can be obtained from the proper orientation of monocrystal in a magnetic field), and such data, up to my best knowledge, are not available for C–S–H gel. However, the measurement of CSA for non-crystalline samples is principally possible with certain two dimensional NMR techniques, thus there is a chance, that such experiments will be performed for hydrated cements and my theoretical results will become helpful in the interpretation of such data.

2.2.2 Polymorphism and doping in crystalline components of high alumina cements – periodic DFT calculations [H3, H4]

The next topic of my studies on physics and chemistry of cements, proposed by the experimental group of prof. Miguel Aranda (Malaga University, ALBA synchrotron), was cry-

[16] $\gamma = \frac{\frac{1}{n}\sum_{i=1}^{n}(x_i-\overline{x}_i)^3}{(\frac{1}{n}\sum_{i=1}^{n}(x_i-\overline{x}_i)^2)^{(3/2)}}$, (in silica tetrahedra $n = 4$).

[17] Löwdin charges are in the ranges: (i) 1.20–1.35, for Si atoms, (ii) (-0.5)–(-0.7), for dangling O atoms, (iii) (-0.3)–(-0.5), for bridging O atoms (in Si–O–Si/H positions).

stalline aluminates, being either the primary components of high alumina cements or the secondary phase in ordinary Portland cements.

I performed the periodic DFT/PBE calculations using SIESTA code,[18] which utilizes localized numerical basis sets and norm-conserving pseudopotentials.[10] I applied the basis set denoted by the SIESTA authors, in analogy to Gaussian sets, as double-zeta polarized one, and the fineness of the grid, used for the electron density calculations, corresponded to plane-wave cutoff energy of 400 Ry.

The first work [**H3**], where I was the main author of the computational part, was dedicated to structural studies on ye'elimite (YEL), the main component of hydrated sulfoaluminate cements. The latter group of cements has attracted much attention in recent years as the alternative for Portland cement, due to such desirable properties as lower energy demands for manufacturing, faster setting, and high chemical resistance.[19] YEL, being both component of cements and occurring naturally as mineral, structurally belongs to the sodalite (SOD) family. SOD is the aluminosilicate crystallizing in a regular system ($P\underline{4}3n$), with the unit cell composition being $Na_8[Al_6Si_6O_{24}]Cl_2$. SOD structure consists of truncated cuboctahedra units, called SOD units, which vertices are determined by the positions of Si and Al atoms, the latter being coordinated tetrahedrally by O atoms. The diameter of these cubooctahedral units, called SOD cages, is about 7 Å. SOD cages are centered with Cl^- anions, whereas Na^+ cations occupy positions near the hexagonal faces of these units. SOD topology remains stable for a wide spectrum of stoichiometry, hence many solids exist, which structure can be formally derived from SOD by the substitution of Na^+ cations (by other metal cations with low charge), Cl^- anions (*e.g.* by. other halides, S^{2-}, SO_4^{2-}), T atoms (e. g. by B, P, Ga), or even O atoms (with N or Cl).[20] There are many mechanisms able to change the space group of SOD type crystals without breaking its topology (partial rotation or deformation of TO_4 units, distribution of various elements between T sites, occlusion of low symmetry molecules within SOD cages), consequently the lattice symmetry may differ from the ideal SOD symmetry, actually, it does not even necessarily remain within the cubic system.

YEL is SOD analogue having all T sites occupied by Al atoms, the unit cell composition being $Ca_8Al_{12}O_{24}(SO_4)_2$, and the assumed space group of YEL is cubic $I\underline{4}3m$. However, the latter space group has been questioned and several alternative refinements of YEL structure were proposed, tetragonal and orthorhombic. The neutron diffraction results, obtained in the experimental part of briefed work [**H3**] showed that the stable YEL structure at room temperature is the orthorhombic one belonging to $Pcc2$ space group and having the unit cell twice larger than in the case of cubic cell. At the elevated temperature (470 °C) the phase transition to (pseudo)cubic structure occurs. In order to study relative energetic stability of various YEL polymorphs I performed DFT/PBE geometry optimization for several models. As the starting points I used several experimental structures taken from literature: (i) cubic $I\underline{4}3m$, (ii) orthorhombic $Pcc2$ (obtained in the experimental part of discussed work [**H3**]), (iii) tetragonal $P\underline{4}c2$,[21] as well as (iv) the structures obtained by distortion of the basic regular structure (*e.g.* by rotating SO_4^{2-} anion). Moreover, for the optimized models I computed energies of the unit cells expanded and contracted around

[18] J. M. Soler *et al.*, *J. Phys.: Condens. Matter* **2002**, *14*, 2745-2779.

[19] M. C. G. Juenger, F. Winnefeld, J. L. Provis, J. H. Ideker, *Cem. Concr. Res.* **2011**, *41*, 1232-1243.

[20] W. Depmeier, *Rev. Mineral. Geochem.* **2005**, *57*, 203-240.

[21] Structure $I\underline{4}3m$ YEL: H. Saalfeld, W. Depmeier, *Krist. Tech.* **1972**, *7*, 229; $P\underline{4}c2$: Z. Peixing *et al.*, *Proceeding of 9th International Congress on the Chemistry of Cement* **1992**, *1*, 201-208.

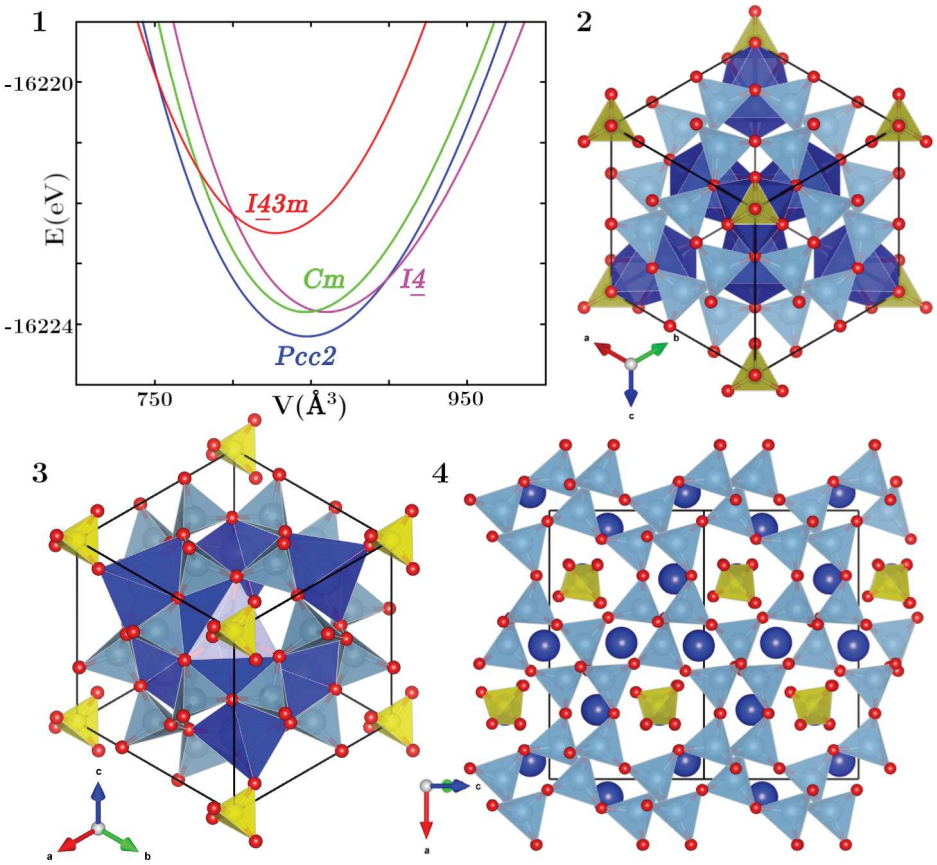

Figure 4: *DFT/PBE results for ye'elimite (YEL): (1) electron energy plotted in function of unit cell volume for different YEL polymorphs, (2) the optimized cubic structure ($I\underline{4}3m$), (3) tetragonal ($I\underline{4}$), and (4) the most stable orthorhombic ($Pcc2$) polymorph, with the unit cell twice larger than the cubic cell. The elements coloring: S–yellow, Ca–dark blue, Al–light blue, O–red.*

the minimum energy structure and fitted these data to Murnaghan formula for energy–volume curve.[22]

The optimized structures and energy–volume curves are shown in Fig. 4. The orthorhombic $Pcc2$ structure appeared to be the most stable YEL polymorph in agreement with experimental data. Tetragonal $P\underline{4}c2$ structure converged to the aforementioned $Pcc2$ one. It should be noted, that orthorhombic $Pcc2$ unit cell has parameters close to these reported for tetragonal one ($a \approx b$), which could explain apparently erroneous refinement of YEL structure as $P\underline{4}c2$. Moreover, using distorted geometries of the cubic cell as the starting points, I found two new structures having intermediate energies between the values for orthorhombic and cubic polymorphs, namely tetragonal $I\underline{4}$ and monoclinic Cm. The tetragonal unit cell has parameters similar to cubic cell ($c \approx b = a$), which suggest, that the cubic YEL polymorph observed at high temperature may be indeed pseudocubic structure with lower symmetry. As shown in Fig. 4 energy–volume curve of the most stable $Pcc2$ structure crosses the curves of $I\underline{4}3m$ and $I\underline{4}$ polymorphs, suggesting that the phase transition to the latter species can be achieved by increasing or decreasing the pressure.

[22] F. D. Murnaghan, *Proc. Natl. Ac. Sci.* **1944** *30*, 244-247. The following equation of state were used: $E(V) = E(V_0) - \frac{B_0 V_0}{B_0'-1} + \frac{B_0 V}{B_0'}\left(\frac{(V_0/V)^{B_0'}}{B_0'-1} + 1\right)$.

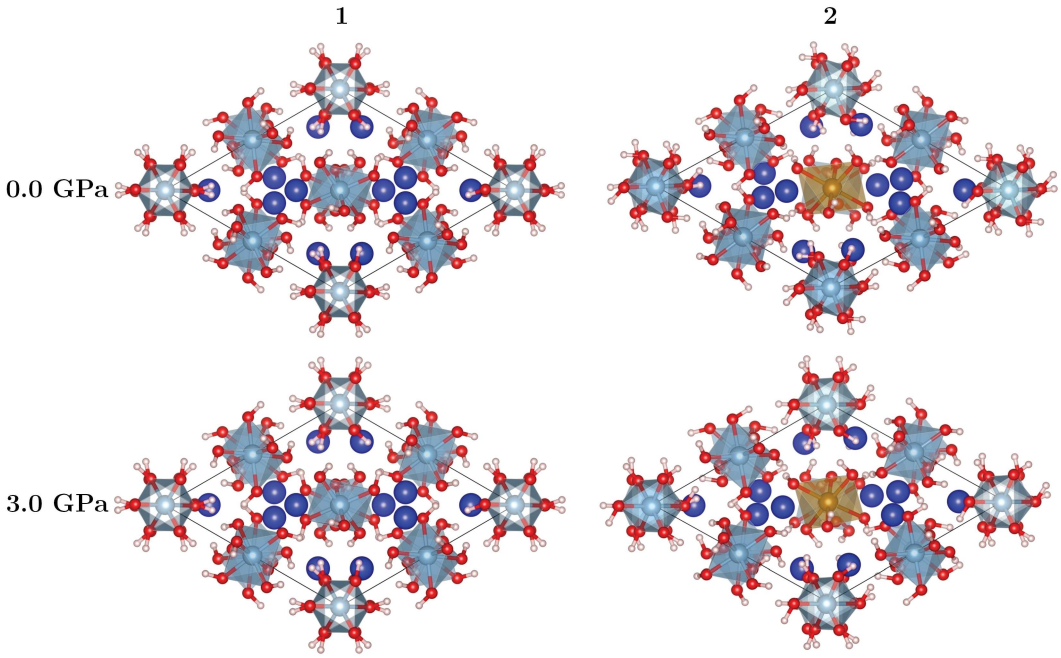

Figure 5: *The optimized at DFT/PBE level structures of KAT: (1) stoichiometric one ($Ca_3Al_2(OH)_{12}$) and (2) doped one Fe ($Ca_3Al_{1.7}Fe_{0.3}(OH)_{12}$), without external pressure and under hydrostatic pressure of 3 GPA. The elements coloring: Ca–dark blue, Al–light blue, O–red, H–white, Fe–brown (Ca–O bonds not depicted for the better clarity of figure). The projection is in the [010] direction of the primitive cell of the body-centered cubic lattice.*

Predicted computationally monoclinic *Cm* polymorph has not been observed experimentally yet: however, the course of its energy–volume curve shows that this phase cannot be obtained simply by expansion or compression of the most stable orthorhombic phase. The ideal cubic symmetry in YEL is possible only if the threefold symmetry axis of SO_4^{2-} tetrahedra coincide with the sixfold axis of SOD cages. Such arrangements lead, however, to unfavorable electrostatic interactions in an ionic lattice (SO_4^{2-} tetrahedra would share faces with CaO_6 octahedra), therefore, lattices with lower symmetry, with sulfate anions rotated with respect to aluminate skeleton and the latter being expanded, are energetically more favorable.

The second work on crystalline aluminates in cement, where I was the main author of the theoretical part, dealt with the change in compressibility of katoite (KAT) upon the doping with Fe^{3+} ions. KAT, $Ca_3Al_2(SiO_4)_{(3-x)}(OH)_{4x}$, $1.5 \leq x \leq 3$, is the mineral of the garnet group, crystallizing in the cubic system ($Ia\underline{3}d$).[23] KAT is the secondary phase of the hydrated Portland cements, whereas its silicon-free, purely aluminum form (C_3AH_6 in cement notation) is the main product of hydration of calcium aluminate cements.[24]

Bulk moduli of both silicon-free KAT (C_3AH_6), and Fe^{3+} doped one ($Ca_3Al_{1.7}Fe_{0.3}(OH)_{12}$) were measured in the experimental part of summarized work [**H4**] : Fe^{3+} ion is an impurity frequently substituting Al^{3+} in various aluminates and aluminosilicates. The starting point for the DFT/PBE calculations, based on crystallographic data, was the primitive unit cell of KAT with $Ca_{12}Al_8(OH)_{48}$ composition and being twice smal-

[23] G. A. Lager, W. G. Marshall, Z. Liu, R. T. Dowes, *Am. Mineral.* **2005**, *90*, 639-644.

[24] E. L'Hôpital, B. Lothenbach, G. Le Saout, D. Kulik, K. Scrivener, *Cem. Concr. Res.* **2015**, *75*, 91-103; W. E. Lee *et al.*, *Int. Mater. Rev.* **2001**, *46*, 145-166.

ler than the body-centered cubic cell. To described doped KAT, one of Al atoms was replaced by Fe one, giving Fe loading only minutely smaller than the experimental one. First I optimized stoichiometric and Fe KAT, then I run a series of constant volume optimizations for the cells stressed and expanded around the equilibrium volumes. For the latter data I fit energy–volume curves using the thirdr-order Murnaghan formula and obtained bulk moduli B. Moreover, I optimized both variants of KAT under hydrostatic pressure of 3GPa. The computed values of B are about 20% lower than experimental ones (which can be ascribed to underestimating the bond strength by gradient exchange–correlation functional), however, the lowering of B value in Fe doped KAT is qualitatively reproduced. The compression of both KAT variants is associated with bond contractions, without the relative displacements of coordination polyhedra, as shown in Fig. 5. The analysis of bonding pattern in equilibrium and compressed structures of studied KAT models revealed, that the replacement of $Al(OH)_6^{3-}$ octahedron by $Fe(OH)_6^{3-}$ one increased the network of hydrogen bonds (the shortening of mean hydrogen bond lengths by 0.3 Å and increase in the mean number of these bonds per H atom over one), at the expense of weakening of Ca–O bonds (the mean length of the latter bonds increases by 0.02 Å and the mean Ca–O coordination number dropped below 8). The latter effect overwhelmed, hence the increased compressibility of Ca–O polyhedra lowered the overall B value in Fe doped KAT. The mean shortening of Ca–O bonds in the stoichiometric and doped KAT under the pressure of 3 GPa amounts to 0.025 and 0.040 Å, respectively, the remaining bonds contract under pressure uniformly. The analysis of Hirshfeld charges showed that the charge flow in pressurized KAT lattices occurred mainly between Ca and O atoms.

2.2.3 The computational determination of structural, optical, and magnetic properties of ultramarine pigments with periodic and cluster modeling [H5, H8]

Ultramarines (UM) are one of the most commonly applied pigments, known since ancient times as mineral lazurite and manufactured since the 19th century.[25] UM are SOD type aluminosilicates (see 2.2.2) Their intense blue color stems from $S_3^{\bullet -}$ radical anions replacing Cl^- anions within SOD structure. Apart from the aforementioned blue $S_3^{\bullet -}$ chromophore, SOD cages can be occupied by yellow $S_2^{\bullet -}$ chromophore, as well as crudely characterized red chromophore, usually ascribed to tetrasulfur molecule or anion. There are also known synthetic analogues of UM, where aforementioned colored polysulfur species are occluded in the cages of aluminosilicates other than SOD.[26] Despite a large number of experimental works on UM, as well as theoretical studies on $S_3^{\bullet -}$ radicals (either the isolated ones or within small cluster models with a few cations),[27] the computational periodic results, somewhat surprisingly, have not been reported until now. With my studies I aimed to fill this gap, the goal I accomplished successfully, and the effect of my efforts are two unassisted papers. The first paper ([**H5**]) contains the analysis of structural and spectroscopic properties of blue UM, achieved with periodic and large cluster models, and the confrontation of such results with the available experimental data. In this work, I presented also preliminary results for the yellow $S_2^{\bullet -}$ chromophore, which experimental characterization was the subject of controversy. In the second work ([**H8**]) I managed to clarify the identity of chromophore occurring in the synthetic red UM, up to date variously identified as one of the isomers of either radical $S_4^{\bullet -}$ anion or neutral S_4 molecule.

[25] D. Reinen, G.-G. Lindner, *Chem. Soc. Rev.* **1999**, *28*, 75-84.

[26] S. Kowalak, A. Jankowska, S. Zeidler, A. B. Więckowski *J. Solid State Chem.* **2007**, *118*, 1119-1124.

[27] M. W. Wong, *Top. Curr. Chem.* **2003**, *231*, 1-29; R. Steudel, *Top. Curr. Chem.* **2003**, *231*, 127-152; R. Steudel, T. Chivers, *Chem. Soc. Rev.* **2019**, *48*, 3279-3319.

For geometry optimization and Γ phonon calculations at the DFT level, I employed QUANTUM ESPRESSO code, [7] with gradient PBE functional,[9] ultrasoft Vanderbilt pseudopotentials[28] and plane-wave cutoff energy of 40 Ry. For Brillouin zone sampling, I applied uniform 2×2×2 k-points mesh in [**H5**] study, for [**H8**] paper, I found Γ point calculations being enough.

In order to determine spectroscopic properties of interest, I cut large cluster models from the optimized periodic structures and, for this category models, I performed all-electron calculations with ORCA package[29] for molecular calculations, using atom-centered Gaussian basis sets. The advantages of such basis sets are: (i) the explicit treatment of core electrons, owing to rather good representation of oscillating radial part of orbitals in the vicinity of nuclei by a small number of basis functions,[30] and (ii) relatively low computational cost of two electron integrals, notably the exchange ones. The latter enables effective implementation of more advanced, with respect to (semi)local DFT variants, electronic structure methods, such as hybrid DFT functionals (containing the admixture of Hartree-Fock exchange) or various correlated methods utilizing wavefunction functional approach (referred to as "quantum chemistry methods") in Gaussian functions employing codes. In my cluster DFT studies, I used triple-zeta quality Gaussian basis sets with polarization functions for the valence shells and additionally diffusion functions on S atoms within anionic radicals. I employed hybrid B3LYP functional[31] for the calculations of g tensor in the electron paramagnetic resonance (EPR) spectroscopy. The vertical electronic excitation energies were computed at time dependent DFT (TDDFT) level with asymptotically corrected hybrid functionals: CAM–B3LYP[32] in [**H5**] study and LC–BLYP[33] in [**H8**]. It is worthwhile to note that only the latter class of functionals deliver excitation energies comparable to UV-Vis experiments for cluster models, other functionals (gradient or simple hybrid) predicted plenty of apparently unphysical excitations in the optical region, stemming from the charge transfer between S atoms and the lattice O atoms. Additionally in [**H8**] work I performed electronic structure calculations for $S_4^{\bullet -}$ and S_4 species using correlated methods of quantum chemistry, namely CCSD(T) (the variant of coupled cluster approach) and CASSCF+NEVPT2 (the variant of complete active space self-consistent field method with second-order perturbation corrections), using quadruple-zeta basis sets, augmented with diffusion functions for $S_4^{\bullet -}$ anion.

In my studies on blue UM ([**H5**]) I performed DFT/PBE geometry optimization for twelve periodic models in total, belonging to three types of unit cell stoichiometry: (i) $Na_8(S_3^{\bullet -})$Cl-sod, (ii) $Na_7(S_3^{\bullet -})$-sod, and (iii) $Na_8(S_3^{\bullet -})_2$-sod, where sod = $(Si_6Al_6O_{24})^{6-}$, and of the different initial orientation of $S_3^{\bullet -}$ radical within SOD cage. These models converged eventually to ten inequivalent local minima of energy (for a given unit cell composition the energy differences did not exceed a few kJ/mol per unit cell), of which six the most stable ones (*i.e* two models per each considered stoichiometry) I examined in greater detail and used for subsequent cluster modeling. Exemplary models are presented in Fig. 6. S–S bond lengths amount to about 2.0 Å, and the valence S–S–S angles are in the range of 108°–114°, thus being only minutely lower than the corresponding values predic-

[28] D. Vanderbilt, *Phys. Rev. B* **1990**, *41*, 7892-7895.

[29] F. Neese, *Wiley Interdiscip. Rev.: Comput. Mol. Sci.* **2018**, *8*, e1327.

[30] At least for the light atoms, for the heavier ones (Z>40) one need to either apply effective core potentials, including relativistic effects for core electrons or explicitly use relativistic variants of quantum mechanics.

[31] A. D. Becke, *J. Chem. Phys.* **1993** *98*, 1372-1377; C. Lee, W. Yang, R.G. Parr, *Phys. Rev. B* **1988**, *37*, 785-789.

[32] T. Yanai, D. P. Tew, N. C. Handy, *Chem. Phys. Lett.* **2004**, *393*, 51-57.

[33] Y. Tawada, T. Tsuneda, S. Yanagisawa, T. Yanai, K. Hirao, *J. Chem. Phys.* **2004**, *120*, 8425-8433.

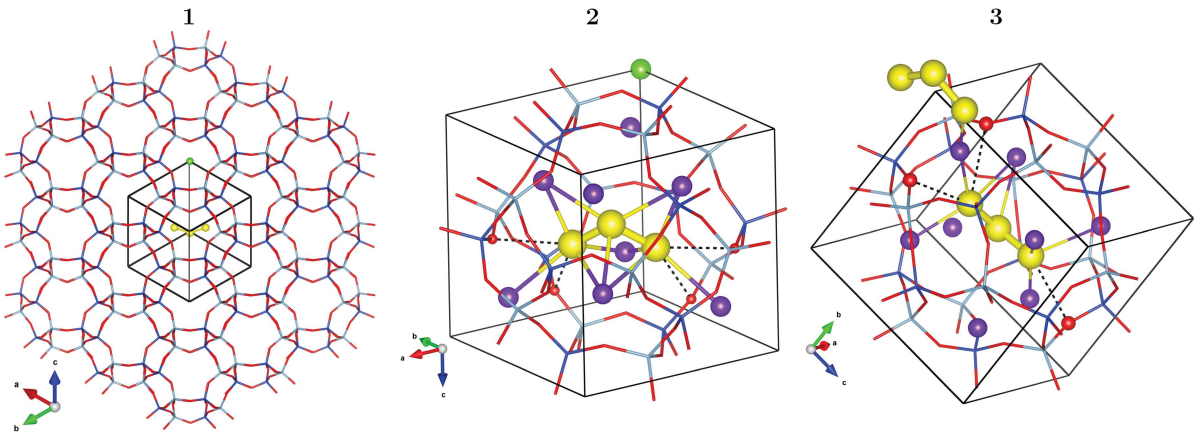

Figure 6: *The structures of blue ultramarines: (1) the general view of the cubic sodalite-type lattice with embedded ion: for clarity Na^+ ions omitted and $S_3^{\bullet-}$ ions shown only for single cell, along with the DFT/PBE optimized models: (2) the most stable model of $Na_8(S_3^{\bullet-})Cl$-sod stoichiometry, (3) the most stable $Na_8(S_3^{\bullet-})_2$-sod model, where sod = $(Si_6Al_6O_{24})^{6-}$. The elements coloring: S–yellow, Na–purple, Si–dark blue, Al–light blue, O–red, H–white, Cl–green.*

ted at DFT/PBE level for the isolated $S_3^{\bullet-}$ radical (2.01 Å and 116.3°), and quite close to the available experimental data obtained from the X-ray absorption spectroscopy (2.05 Å and 110°).[34] $S_3^{\bullet-}$ ions interact with Na^+ ones mainly via the terminal S atoms, with Na–S distances being about 2.8 Å, the distances between terminal S atoms and the lattice O atoms are no shorter than 3.1 Å. The nearest distances between the adjacent $S_3^{\bullet-}$ ions (*i.e.* their periodic images or two radicals in a single unit cell) are always greater than 6 Å. It should be noted that the geometries of $S_3^{\bullet-}$ radicals in UM have not been resolved crystallographically: these anions can adopt various orientations within SOD cages and/or be partially replaced by other anions (*e.g.* Cl^-, SO_4^{2-}, S^{2-}), hence they do not give clear diffraction patterns.

The analysis of Γ point phonons showed that $S_3^{\bullet-}$ vibrations in UM are fairly well separated from the lattice oscillations and can be interpreted as three normal modes of nonlinear three-atomic molecule. Harmonic DFT/PBE frequencies are in very good agreement with experimental Raman values,[35] being 280, 540 and 580 cm^{-1} for bending, symmetric and antisymmetric stretching modes, respectively (all Raman active for C_{2v} symmetry).[25] The vibrations of $S_3^{\bullet-}$ ions in UM exhibit frequencies about 20-40 cm^{-1} higher than the corresponding oscillations predicted for gas-phase radical, which stems from the small shortening of S–S bonds in UM. In some models, there are also additional lattice vibrational modes involving non-negligible displacement of S atoms.

The interpretation of electron paramagnetic resonance (EPR) and ultraviolet–visible absorption spectroscopy (UV-Vis) was based upon all-electron DFT calculations in localized basis sets for cluster models. Routinely I performed such calculations for cluster models representing a single SOD cage and having formulas $[(S_3^{\bullet-})Na_{(6-8)}(H_2O)_{(15-20)}]^{(5-7)+}$.

[34] M. T. Weller, *J. Chem. Soc., Dalton Trans.* **2000**, 4227-4240.

[35] The direct comparison of computed harmonic frequencies with experimental anharmonic ones is strictly speaking incorrect, however, anharmonic effects are often negligible for strong covalent bonds. Moreover, as gradient functionals slightly underestimate bond strength and consequently harmonic frequencies, the latter error may work effectively as an anharmonic correction. For $S_3^{\bullet-}$ anharmonicity is small indeed: J. A. Tossell, *Geochim. Cosmochim. Acta* **2012**, *95*, 79-92.

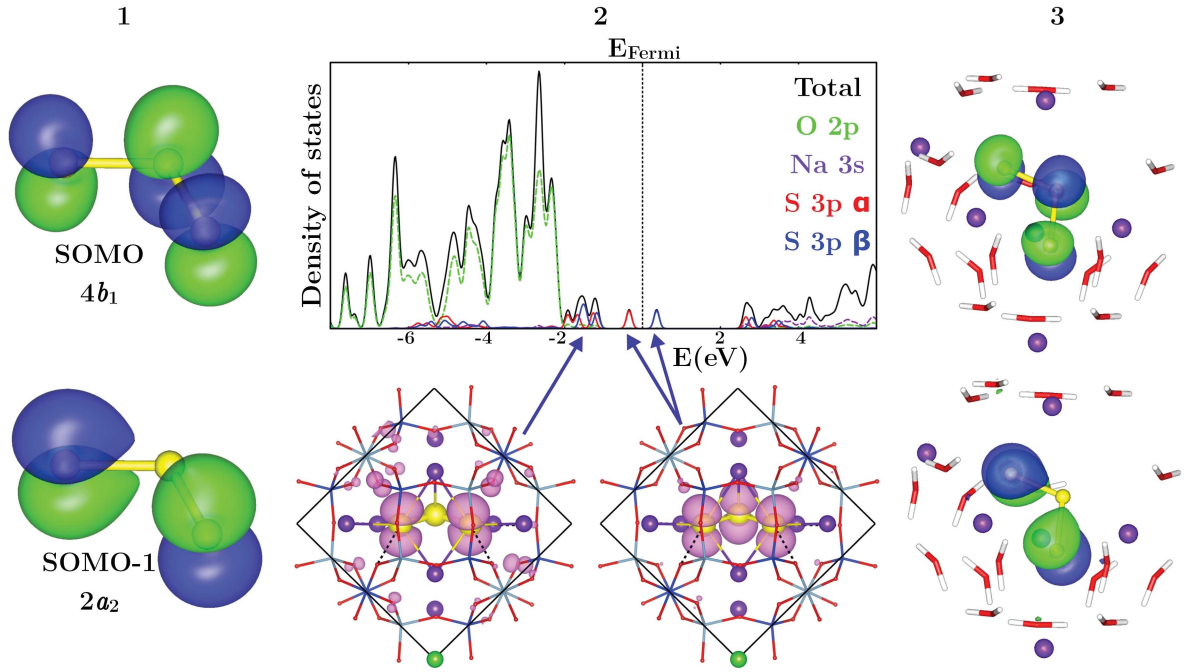

Figure 7: *The comparison of electronic properties of $S_3^{\bullet -}$ radicals in various models: (1) molecular orbitals for the isolated ion, singly occupied molecular orbital (SOMO) and the next highest doubly occupied molecular orbital (SOMO-1), irreducible representations given for C_{2v} symmetry, (2) density of states, total and projected on atomic states, for periodic ($Na_8S_3^{\bullet -}$ Cl-sod) model of ultramarine, with depicted contributions from singly occupied and the highest doubly occupied crystal orbitals, along with the contours of squared* Γ *point orbitals, (3) SOMO and SOMO-1 for cluster model, cut from the aforementioned periodic one The elements coloring: S–yellow, Na–purple, Si–dark blue, Al–light blue, O–red, H–white, Cl–green.*

Apart from the single radical, each model contained Na^+ cations and the lattice O atoms of SOD cage, saturated with H atoms put along the directions of O–Si/Al bonds within periodic UM. Test calculations performed for the cluster consisting of the whole SOD cage ($[(S_3^{\bullet -})Na_8Si_{12}Al_{12}H_{24}O_{60}]^{5-}$, with H atoms saturating terminal O atoms) showed,that further increase in the size of the model did not affect the results.

The paramagnetic properties of $S_3^{\bullet -}$ are determined by singly occupied molecular orbital (SOMO), belonging to $4b_1$ irreducible representation for C_{2v} symmetry of anion, whereas the optical properties depend additionally on the orbital lying below SOMO (SOMO-1), transforming according to $2a_2$ representation: the electronic excitation about 600 nm, responsible for the intensive blue color of discussed chromophore has predominantly $4b_1 \rightarrow 2a_2$ character, both orbitals are shown in Fig. 7. The electronic structure of isolated and embedded in SOD lattice $S_3^{\bullet -}$ anions is similar: the aforementioned $S_3^{\bullet -}$ frontier orbitals are rather well separated from the SOD lattice states both spatially and in energy scale, hence the interaction between them is small. The only optical transitions of large intensity, as predicted at DFT/CAM-B3LYP level for cluster models, are the transitions with predominantly $4b_1 \rightarrow 2a_2$ character within the embedded $S_3^{\bullet -}$ radical. The computed wavelengths (580-645 nm) are in fine agreement with experimental ones (595-620 nm).[25,27] The only exception is the model with the radical the most distorted from the ideal C_{2v} symmetry (S–S bond length being 1.987 and 2.019 Å), with SOMO looking unlike $4b_1$

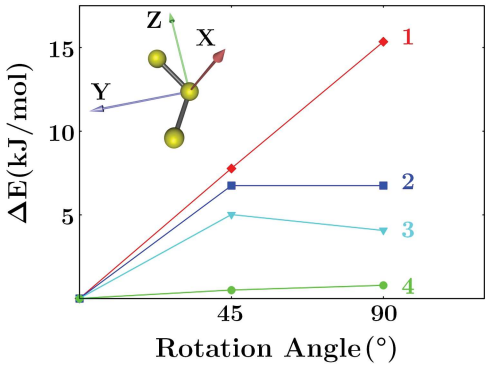

Figure 8: *The estimation of rotation energy (ΔE) of $S_3^{\bullet-}$ radical along the Y-axis in the most stable UM models of stoichiometry: (1) $Na_8(S_3^{\bullet-})Cl$-sod, (2) $Na_7(S_3^{\bullet-})$-sod and (3) $Na_8(S_3^{\bullet-})_2$-sod. Additionally (4) the energy of $S_2^{\bullet-}$ rotation along the arbitrary axis perpendicular to S–S bond in $Na_7(S_2^{\bullet-})$-sod model presented. The energies of optimized structures are taken as zero level for each model.*

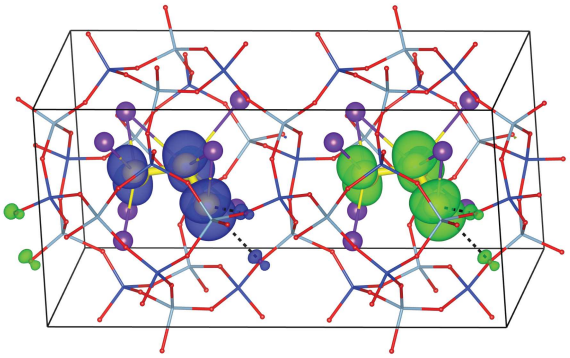

Figure 9: *The spin density for "antiferromagnetic" solution in $Na_7S_3^{\bullet-}$-sod model, the supercell obtained by doubling the initial cell in the direction corresponding to the shortest distance between S atoms belonging to periodic images of $S_3^{\bullet-}$ radical (6.405 Å).*

orbital of the symmetrical anion (the discussed orbital has bonding and antibonding component along the shorter and longer bond, respectively), and SOMO-1→SOMO transition shifted toward the shorter wavelengths (537 nm). Indeed, certain experimental studies on blue UM reported the presence of satellite bands around 540 nm,[36] which can be tentatively ascribed to strongly distorted from C_{2v} symmetry $S_3^{\bullet-}$ ions upon the discussed DFT results.

The principal g tensor components, hence its trace g_{iso}, computed at DFT/B3LYP level[37] are nearly identical for the isolated and embedded radicals:$g_{xx} = 2.002$, $g_{yy} = 2.038$, $g_{zz} = 2.059$, ($\pm.005$), the axis orientation is shown in Fig. 8. DFT/B3LYP g_{iso} (2.032 ± 0.001) agree well with the experimental values (typical reported value of g_{iso} is 2.029).[27] EPR measurements for UM typically revealed isotropic signal at room temperature, resolvable into components only at a lower temperature, with some paramagnetic sites retaining isotropic signal even then.[38] The averaging of the EPR signal was explained either as the result of exchange coupling between the neighboring spin centers[38] or as the effect of $S_3^{\bullet-}$ mobility within SOD cages.[36] I verified both explanations at the computational level. First, for the periodic models with two spin centers per cell ($Na_8(S_3^{\bullet-})_2$-sod and doubled cell of $Na_7(S_3^{\bullet-})$-sod) I calculated the energy of states with parallel spins ("ferromagnetic" triplet) and antiparallel spins ("antiferromagnetic" singlet with broken spin symmetry), see also Fig. 9. The energies of both states were identical (up to 10^{-3} kJ/mol accuracy), which shows that there is no interaction between the adjacent spin centers in UM. Second, to roughly estimate the mobility of $S_3^{\bullet-}$ anions in SOD cages, for three selected UM models I checked the difference in lattice energy upon the rotation of radical along the Y-axis of g tensor (corresponding to C_2 axis in ideal C_{2v} symmetry) without the relaxation of the rest of the lattice. Because g_{xx} and g_{zz} deviate the most from

[36] K. Raulin *et al.*, *Phys. Chem. Chem. Phys.* **2011**, *13*, 9253-9259.
[37] The values obtained at DFT/PBE level are very similar.
[38] D. Arieli, D. E. W. Vaughan, D. Goldfarb, *J. Am. Chem. Soc.* **2004**, *126*, 5776-5788.

the mean g_{iso} value, one can assume that rotation along the Y-axis is the most important for signal averaging. The estimated rotation energy barriers, presented in Fig.8, shows quite large dispersion (between 5-15 kJ/mol), which implies that the mobility of $S_3^{\bullet -}$ within SOD cages should also vary, depending on the local coordination or radical by Na^+ cations. The above results showed that the factor affecting different averaging of EPR signal are differences in the dynamics of $S_3^{\bullet -}$ radicals, not the exchange coupling between the nearest spin sites.

In the last part of this study I focused on periodic and cluster UM models containing yellow $S_2^{\bullet -}$ chromophore, which absorbs the light at 400 nm wavelength and frequently accompanies trisulfur radicals in UM.[27] This species was found to be much more problematic for DFT due to its multireference character, which cannot be reproduced well within a single determinant Kohn–Sham approximation. An open shell in the isolated $S_2^{\bullet -}$ ion is doubly degenerated $\pi^\star(3p_x, 3p_y)^3$ orbital, which splits upon the embedding in UM lattice. The size of this splitting, determining both visible light absorption and g tensor components, strongly varied, depending on both adopted model (different local coordination by Na^+ ions) and employed exchange–correlation functional, making DFT quantitative predictions dubious. Nevertheless, the important qualitative result is observation, that optical and magnetic properties of $S_2^{\bullet -}$ radical are much more sensitive to the environment than it was in the case of $S_3^{\bullet -}$ ion. It cannot be excluded, that $S_2^{\bullet -}$ may contribute to more than one EPR signal, which possibly can be one of the sources of difficulties with experimental identification of this radical.[36] The estimated rotation energy of $S_2^{\bullet -}$ ion within $Na_7S_2^{\bullet -}$-sod model is close to zero, showing that even in not too high temperatures EPR signal of this radical should be dynamically averaged.

The second computational study of mine on UM ([**H5**]) intended to solve the puzzle of the identity of red chromophore absorbing light at about 520 nm wavelength, which is responsible for the coloration of so called red UM (actually, their colors are various shades of pink and violet, due to the presence of residual blue $S_3^{\bullet -}$). Upon the fragmentary data from resonance Raman spectroscopy and sterical restrictions imposed by SOD lattice (S_n molecules with $n \geq 5$ would not fit into SOD cage) this red chromophore was identified either as a neutral S_4 molecule or $S_4^{\bullet -}$ radical ion.[27] Certain experimental data, as well as advanced quantum chemical calculations[39] for gas-phase tetrasulfur pointed at the planar isomer of neutral S_4 molecule with C_{2v} symmetry as red chromophore, however, the assignment of $S_4^{\bullet -}$ radical as the discussed chromophore in UM remains common in experimental works. The purpose of my research was to settle this issue by performing electronic structure calculations for the realistic models of UM, consisting of $S_4/S_4^{\bullet -}$ species embedded in SOD lattice.

The isomers of S_4 and $S_4^{\bullet -}$, considered by me, are gathered in Fig. 10. The unit cell compositions of periodic models of red UM were as follows: (i) $Na_8S_4(S^{2-})$-sod and $Na_8S_4(Cl^-)$-sod, for SOD lattices with the neutral S_4 molecule embedded, and (ii) $Na_8(S_4^{\bullet -})(Cl^-)$-sod and $Na_7S_4^{\bullet -}$-sod, for lattices with radical anion, (sod = $(Si_6Al_6O_{24})^{6-}$). Overall, I optimized at DFT/PBE level 35 various initial periodic structures, of which 18 the most stable (for a given stoichiometry and tetrasulfur species) I used for further studies.

The most stable isomer for both neutral and charged species in a gas phase was *cis*–C_{2v} one, the second one was *trans*–C_{2h}, both with planar structure. The gas-phase energy difference is quite large in the case of neutral tetrasulfur (*trans* species about 40 kJ/mol less stable than *cis* one), whereas for charged radical these both isomers were practically degenerated (DFT energy difference about 1 kJ/mol). C_{2v} isomer remains the most stable

[39] M. W. Wong, R. Steudel, *Chem. Phys. Lett.* **2003**, *379*, 162-169; J. Fabian, N. Komiha, R. Linguerri, P. Rosmus, *J. Mol. Struct. THEOCHEM*, **2006**, *801*, 63-69.

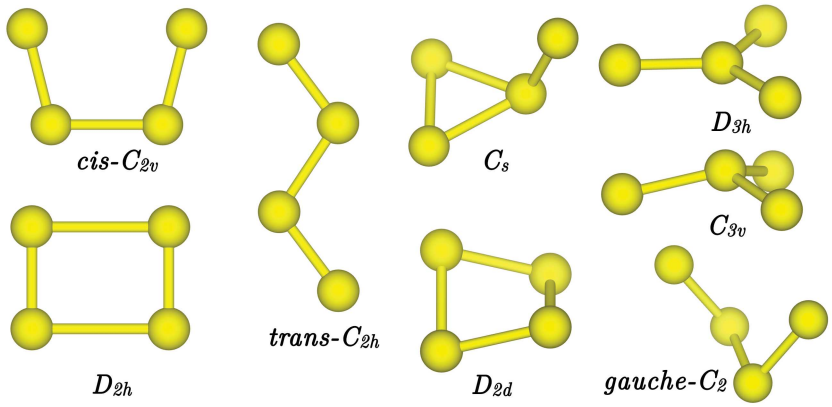

Figure 10: *$S_4/S_4^{\bullet-}$ isomers considered in my work. D_{2h}isomer was found to be a transition state between two pseudorotated C_{2v} ones. Gauche structure (of the ideal C_2 symmetry) was found unstable in a gas phase (depending on the initial torsion it converged to either C_{2v} or C_{2h} planar isomers). Branched D_{3h} and C_{3v} species are predicted stable for the neutral S_4 molecule and $S_4^{\bullet-}$ ion, respectively.*

one for neutral and charged tetrasulfur species encapsulated in SOD cages. However, C_{2h} isomer was strongly destabilized by embedding in the case of neutral S_4, whereas in the case of $S_4^{\bullet-}$ ions none of the initial C_{2h} structures were preserved in the optimization process, undergoing distortion to either C_{2v} or nonplanar *gauche* structure, the latter unstable in a gas phase. Also in one case of embedded neutral S_4 the initial *trans* isomer converged to a *gauche* one.

For the prediction of spectroscopic (UV-Vis and EPR) properties I used cluster models consisting of the whole SOD cage with formulas $[S_4Na_{(7-8)}Si_{12}Al_{12}O_{60}H_{24}]^{(4-6)-}$, where the dangling bonds of O atoms were saturated with H atoms. The most intensive electronic excitations in S_4 and $S_4^{\bullet-}$ species corresponds to electron transition from the highest doubly occupied molecular orbital to the lowest-unoccupied molecular orbital (HOMO→LUMO) or singly occupied molecular orbital (SOMO-1→SOMO), respectively, see also Fig. 11. Similarly to the $S_3^{\bullet-}$ ion case, the relevant frontier orbitals in periodic and cluster models are mainly localized at tetrasulfur moiety and they look alike the corresponding orbitals for the isolated $S_4/S_4^{\bullet-}$ species. The analysis of wavefunction character at DFT and advanced quantum chemistry (CCSD(T), CASSCF+NEVPT2) levels showed mild singlet–triplet instability for S_4 isomers (including *cis*–C_{2v} one), however, this effect is not serious enough to spoil DFT results, which agrees with similar reports from the previous theoretical research.[39] For the neutral S_4 molecule the excitation energies of embedded and free species are very similar, whereas in the case of $S_4^{\bullet-}$ anion, the trapping in SOD lattice shifts excitation energies fairly strong (by $\approx$ 0.5 eV) in comparison to the corresponding gas-phase values. The latter notice confirms the necessity of proper treatment of environment in the description of charged polysulfides.[40] The only S_4 species strongly absorbing light around 500 nm is C_{2v} isomer, among radicals high energy C_s and C_{3v} (depending on the model and level of theory) absorb in this region. The most stable C_{2v} isomer of $S_4^{\bullet-}$ exhibits the strongest absorption the in near-infrared range.

Moreover, for the isolated and embedded in cluster models $S_4^{\bullet-}$ radicals, I computed g tensor principal components. The value of g_{iso} for *cis*–C_{2v} isomer is slightly higher than the corresponding experimental value reported for $S_3^{\bullet-}$ radical in blue UM, however,

[40] R. Steudel, Y. Steudel, *Chem. Eur. J.* **2013**, *19*, 3162-3176.

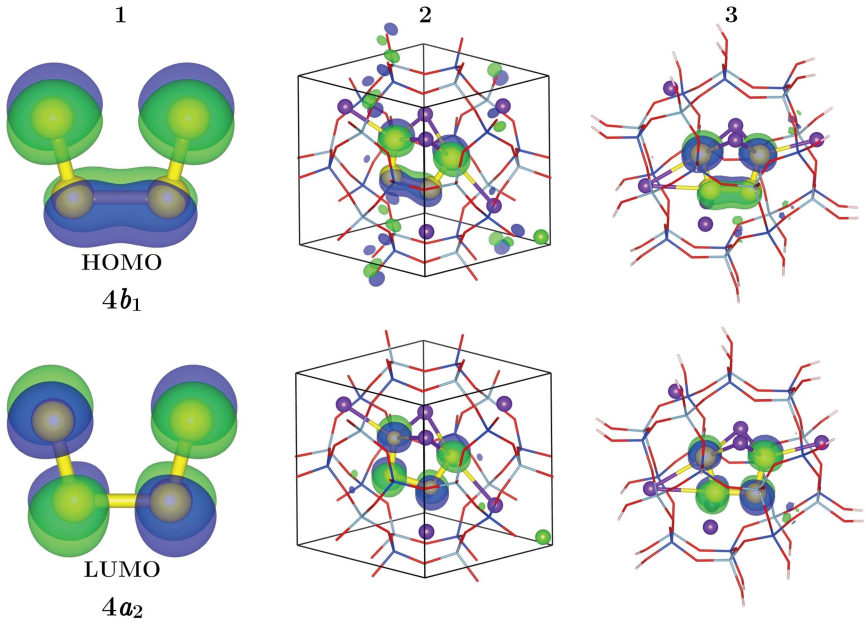

Figure 11: *The frontier orbitals for systems containing cis–C_{2v} S_4 molecule: (1) the highest occupied molecular orbital (HOMO) $4b_1$ and the lowest unoccupied molecular orbital (LUMO) $4a_2$ in the isolated molecule, (2) the corresponding crystal orbitals in periodic Na_7S_4Cl-sod model, and (3) the corresponding orbitals in cluster models, employed for the prediction of electronic excitation energies. In C_{2v} $S_4^{\bullet-}$ radical $4b_1$ orbital is singly occupied. The excitations of $4b_1 \rightarrow 4a_2$ type are the most intensive in these systems.*

the individual g components are very different for both radicals. Also, the principal g tensor components for the remaining $S_4^{\bullet-}$ ions vary strongly, which shows the potential of EPR spectroscopy in the identification of $S_4^{\bullet-}$ isomers.

Among the studied UM periodic models with occluded tetrasulfur species I found the best agreement of Γ point harmonic phonons with experimental resonance Raman data for C_{2v} isomer of S_4 molecule. Red chromophore in UM shows vibrational bands at 675, 655, 410, and 355 cm^{-1}.[41] Upon computational results, these modes can be respectively ascribed to: (i) symmetric stretching of terminal S–S bonds and (ii) its antisymmetric counterpart, (iii) antisymmetric bending, and (iv) middle S–S bond stretching mode in *cis*–C_{2v} S_4, see Fig. 12. It is worthwhile to note, that the last two modes exhibit accidental degeneracy in a gas phase, shifted upon the confinement in SOD lattice. The remaining isomers of $S_4/S_4^{\bullet-}$ usually lack vibrational modes at the high-frequency range (about650 cm^{-1}) and/or in the 300-400 cm^{-1} range.

In discussed research, I showed that the only plausible candidate for red chromophore in UM is *cis*–C_{2v} isomer of the neutral S_4 molecule, thus the assignment of this chromophore to $S_4^{\bullet-}$ radical, still found in recent literature, is incorrect. The hypothetical presence of *cis*–C_{2v} $S_4^{\bullet-}$ ion in UM can be detected by the strong absorption in the near-infrared range and the detailed analysis of the EPR signal. I have shown that the influence of the environment can affect the spectroscopic properties of confined polysulfides. Although the discussed research was focused on UM, some of the obtained results, particularly dealing with charged $S_4^{\bullet-}$ radical, can be helpful in studies on other systems, where such polysulfides are present, *e.g.* metal–sulfur batteries.[27]

[41] R. J. H. Clark, T. J. Dines, M. Kurmoo, *Inorg. Chem.* **1983**, *22*, 2766-2772.

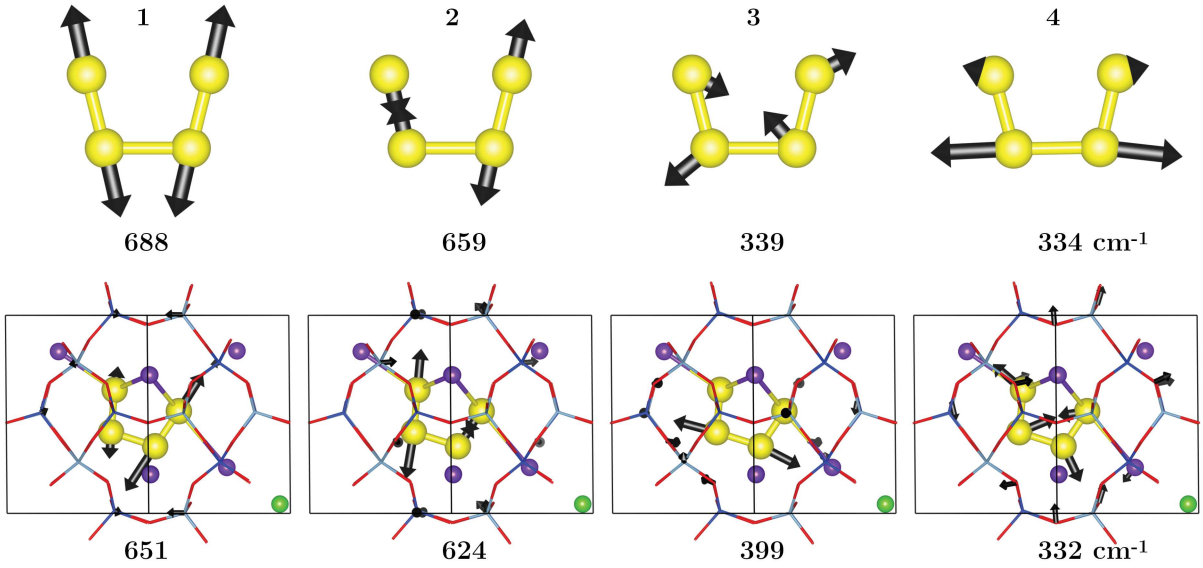

Figure 12: *Four highest vibrational modes for C_{2v} isomer of S_4 molecule in a gas phase (upper panel) and embedded in SOD cage (lower one), as predicted at DFT/PBE level in harmonic approximation: (1) symmetric and (2) antisymmetric stretching of terminal S–S bonds, (3) antisymmetric in-plane bending, and (4) stretching of middle S–S bond.*

2.2.4 The structural characterization and vibrational analysis of Ca_2SiO_4 polymorphs with periodic DFT and MM methods [H6]

Dicalcium orthosilicate, Ca_2SiO_4 (C2S), also known as belite, constitutes approximately 20% of dry Portland cement mass,[42] there is also increasing interest in cements having C2S as their main component.[43] Moreover, there are also known phosphors obtained from C2S matrices doped with lanthanide ions.[44] The interesting feature of C2S, setting it apart from other ternary salts of A_2BX_4 stoichiometry, is the formation of at least five polymorphs in the temperature range of 500–1500°,[45] see Fig. 13. The majority of A_2BX_4 salts has only two polymorphs, low-temperature orthorhombic and high-temperature hexagonal.[46] Other unusual properties of C2S are: (i) decrease in unit cell volumes of high temperature phases with respect to the most stable γ variant, (ii) thermal hysteresis in phase transition cycle, revealing itself in the formation of intermediate β polymorph on cooling from α'_L to γ. C2S polymorphs exhibit different reactivity toward the water, which is an important issue in cement technology. The weakest hydraulic activity is shown by the most stable γ phase, hence one usually attempts to stabilize the more reactive high temperature phases, either by doping (*e.g.* by partial replacement Ca^{2+}/SiO_4^{2-} with other metal cations/oxoanions), or by powdering C2S bulk.

[42] S. Telshow, F. Frandsen, K. Theisen, K. Dam-Johansen, *Ind. Eng. Chem. Res.* **2012**, *51*, 10983-11004.
[43] A. Cuesta, A. Ayuela, M. A. G. Aranda, *Cement Concr. Res.* **2021**, *140*, 106319.
[44] J. S. Kum, Y. H. Park, S. M. Kim, J. C. Choi, H. L. Park, *Solid State Comm.* **2005**, *133*, 445-448; Y. Sato *et al. Angew. Chem. Int. Ed.* **2014**, *53*, 7756-7759; A. Kalaji, M. Mikami, A. K. Cheetham, *Chem. Mater.* **2014**, *26*, 3966-3975.
[45] There are reports about the sixth high-temperature polymorph, denoted as x-C2S: M. Miyazaki, S. Yamazaki, K. Sasaki, H. Ishida, H. Toraya, *J. Am. Ceram. Soc.* **1998**, *81*, 1339-1343. Due to rather scarce, in comparison to other C2S phases, experimental material on this polymorph, I have not studied it.
[46] R. L. Withers, J. G. Thompson, B. G. Hyde, *Crystallogr. Rep.* **1989**, *2*, 27-63.

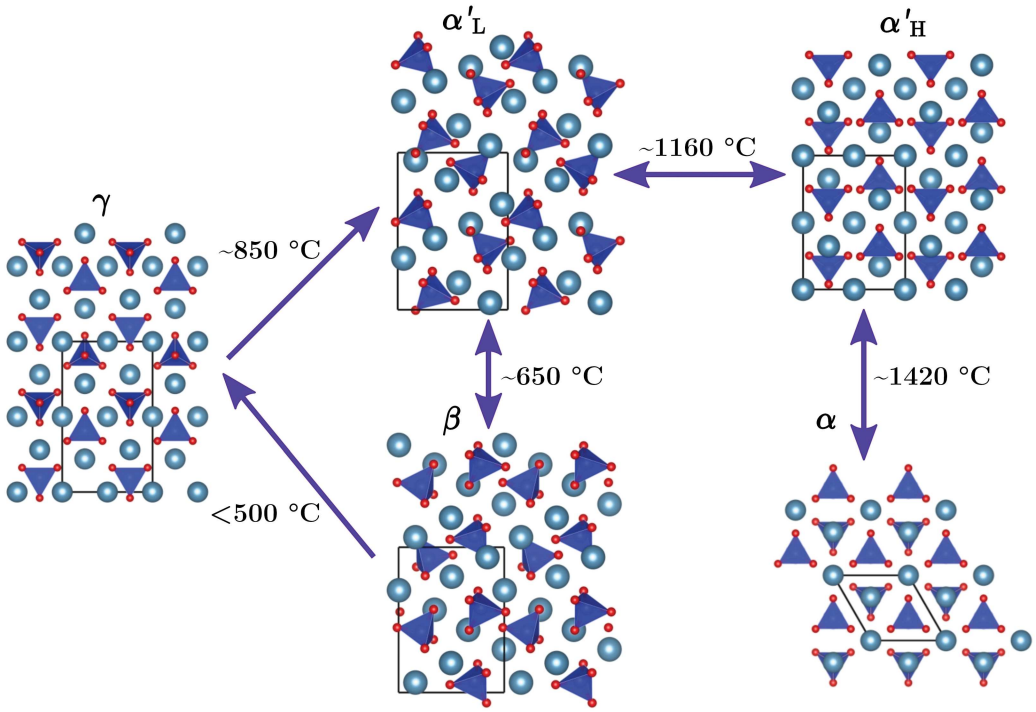

Figure 13: *The structures of five main Ca2SiO4 (C2S) polymorphs, with depicted ordering and temperatures of phase transitions. The projection is in [100] direction, except from α phase, projected in [001] direction. The elements coloring: Ca–light blue, Si–dark blue, O–red.*

In recent years many computational results on C2S has been published,[47] however, each of these works deals with only certain issues of importance for C2S technology (*e.g.* doping, water adsorption), frequently focusing on only selected C2S polymorph (usually on the highly reactive with water β phase) and/or relying on approximate MM methods. Therefore, there is a still long way to more comprehensive understanding of physical chemistry of C2S, surprisingly complicated as for such simple compound, and applying this knowledge in practice. The work discussed below, where I am the main co-author, is the first systematic study on structural, energetic and vibrational properties of all main five C2S polymorphs, relying on both interatomic potentials and electronic structure methods. I focused on modeling of bulk stoichiometric C2S, assuming that understanding such systems, even if somewhat idealized, is a necessary step to clarify more realistic, yet more complicated, issues in the physical chemistry of cements, such as the effect of doping or surface development of nanocrystallites on C2S polymorphs stability.

I performed geometry optimization and calculation of phonon dispersion at (i) DFT level, using QUANTUM ESPRESSO,[7] code, gradient PBE functional,[9] norm-conserving pseudopotentials, [10] plane-wave cutoff energy of 80 Ry and 4×4×4 k-points mesh (lattice constants of considered unit cells are between 5-11 Å), and (ii) at MM level, using

[47] H. Manzano, J. S. Dolado, A. Ayuela, *Acta Mater.* **2009**, *57*, 1666-1674; N. A. Yamnova, N. V. Zubkova, N. N. Eremin, A. E. Zadov, V. M. Gazeev, *Crystallogr. Rep.* **2011**, *56*, 210-220; E. Durgun, H. Manzano, R. J. M. Pellenq, J. C. Grossman, *Chem. Mater.* **2011** *24*, 1262-1267; Q. Wang *et al.*, *Cement Concr. Res.* **2014**, *57*, 28-32; J. Wen *et al.*, *J. Phys. Chem. A* **2015**, *119*, 8031-8039; Q. Wang, H. Manzano, Y. Guo, I. Lopez-Arbeloa, X. Shen, *J. Phys. Chem. C* **2015**, *119*, 19869-19875; P. Guo, B. Wang, M. Bauchy, G. Sant, *Cryst. Growth Des.* **2016**, *16*, 3124-3132; S. K. Saravana *et al.*, *J. Phys. Chem. C* **2018**, *122*, 24235-24245.

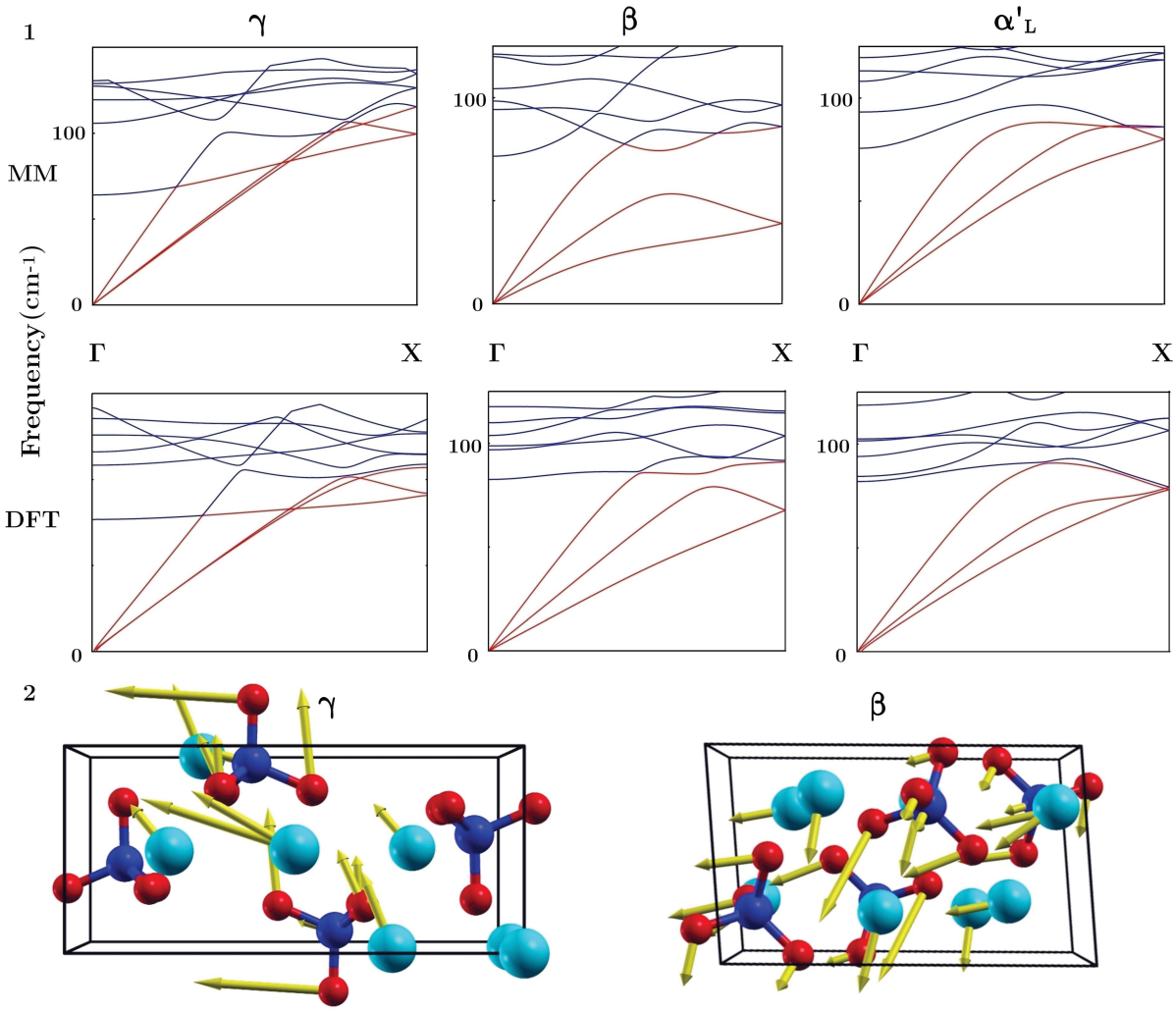

Figure 14: *The harmonic vibrational analysis for three C2S polymorphs stable below 1000 °C, γ, β and α'_L: (1) phonon dispersion curves in Γ-X direction obtained from MM and DFT/PBE calculations, acoustic and optical modes depicted with red and blue colors, respectively, (2) the atomic displacements corresponding to the third lowest phonon branch in X point for γ and β phases: both modes have partially optical character, although in β motions are more in phase. The elements coloring: Ca–light blue, Si–dark blue, O–red.*

implemented in GULP[5] package polarizable interatomic potentials.[6] Initial geometries were based on the available experimental data.[48]

The comparison of the interatomic distances among C2S polymorphs showed that: (i) Si–O bond lengths vary only minutely ($\sim$ 0.01 Å) throughout C2S phases, (ii) the noticeable differences are found for the mean Ca–O distances ($\sim$ 0.1 Å), as well as for Ca–O coordination numbers, which, except for γ polymorph, frequently differ from the "optimal" value of six,[49] (iii) there is clear shortening ($\sim$ 0.1 Å) of distances between Ca^{2+} ions,

[48] Crystallographic structure of C2S polymorphs comes from the following studies: γ and β: W. G. Mumme, R. J. Hill, G. Bushnell-Wye, F. R. Segnit, *Neues Jahrb. Mineral., Abh.* **1995**, *169*, 69-79; α'_L and α: W. G. Mumme, L. Cranswick, B. Chakoumakos, *Neues Jahrb. Mineral., Abh.* **1996**, *170*, 171-188r; α'_H: A. Cuesta, E. R. Losilla, M. A. G. Aranda, J. Sanz, *Cem. Concr. Res.* **2012**, *42*, 598-606.

[49] The value ensuring local electroneutrality in corners sharing CaO_6 octahedra according to the Pauling's rules: L. Pauling, *J. Am. Chem. Soc.* **1929**, *51*, 1010-1026

which was postulated as the factor destabilizing lattice and increasing the reactivity of the high temperature phases of C2S toward the water.[50] The inspection of the experimental and computed structures shows that the phase transitions in C2S are of predominantly displacive nature, connected to the mutual movements of cationic Ca^{2+} and anionic SiO_4^{2-} layers, and the rotations of the latter anions.

Regarding the elastic properties calculated at MM level, a good agreement with experimental data was found for Young moduli, whereas bulk moduli are about one third lower than the experimental values,[51] which can be attributed to the tendency of the applied interatomic potentials to overestimate the unit cell volume.

Phonon analysis showed, that γ, β and α_L polymorphs correspond to the minima of electronic energy (all Γ point frequencies are ≥ 0). The phonon spectra for these three C2S varieties show some interesting features, partially explaining the rich crystallochemistry of C2S. Upon the phonon dispersion curves for Γ–X directions, as shown in Fig. 14, one can see that: (i) the most stable γ phase exhibits coupling between the acoustic and optical modes, indicating susceptibility to phase transition at the elevated temperature, (ii) β and α'_L forms show the noticeable softening (*i.e.* decrease in frequency with the increase of wavevector) of acoustic modes, though of somewhat different character (in β the highest acoustic branch runs in a non-monotonic manner since the middle of Brillouin zone) - this character of phonon dispersion can be related to the tendency of these two polymorphs to form modulated phases and twinning, as well as the observed brittleness of β polymorph. For the high temperature C2S phases the calculations predict the presence of imaginary phonons, specifically, α_H polymorph exhibit imaginary frequencies already at Γ point, whereas in α even the lowest optical phonons are imaginary. The latter result shows that the high temperature C2S polymorphs are not electron energy minima at 0 K and possibly can be free energy minima at nonzero temperature.

2.2.5 The adsorption of CO molecule on Brønsted acidic centers in the mazzite type zeolite – periodic DFT calculations [H7]

Zeolites are the wide group of crystalline, microporous tectoaluminosilicates[52] of general formula $M^{x+}_{x/n}[Al_xSi_yO_{2(x+y)}]\cdot zH_2O$. Zeolites of the given topology of aluminosilicate framework usually remain stable in a rather broad range of Si:Al ratio and for various types of extraframework cations M^{x+}, compensating the charge of substitution Si^{4+} by Al^{3+} ions.[53] Among the zeolites applied in the industrial processes of heterogeneous catalysis and adsorption, acidic zeolites, namely the ones with H^+ ions bound to the lattice O atoms being the charge compensating cations, are particularly important, as they are the most essential catalysts used in the petrochemical industry for the production of fuels.[54]

The last work in recounted scientific achievement, where I was the main author of DFT calculations, focused on the acidic form of mazzite (MAZ) type zeolites [**H8**]. MAZ is the zeolite crystallizing in the hexagonal system, having a one-dimensional system of pores, aligned along the crystal *c* axis, of large diameter (7.2 Å). The interest in MAZ zeolites grew upon the observation, that the adsorption of CO molecules led to exceptionally large (380 cm^{-1}) redshift of OH stretching vibrations.[55] The redshift of OH stretching modes

[50] K. H. Jost, B. Ziemer, R. Seydel, *Acta Crystallogr. B* **1977**, *33*, 1696-1700.

[51] K. Velez, S. Maximilien, D. Damidot, G. Fantozzi, F. Sorrentino, *Cement Concr. Res.* **2001**, *31*, 555-561. C. Remy, D. Andrault, M. Madon, *J. Am. Ceram. Soc.* **1997**, *80*, 851-860.

[52] Tecto(alumino)silicates are (alumino)silicates having each TO_4 tetrahedron linked to four other tetrahedra via its oxygen corners.

[53] J. Weitkamp, *Solid State Ion.* **2000**, *131*, 175-188.

[54] A. Primo, H. Garcia, *Chem. Soc. Rev.* **2014**,*43*, 7548-7561.

[55] R. A. Shigeishi, B. H. Chiche, F. Fajula, *Micropor. Mesopor. Mat.* **2001**, *43*, 211-226.

upon the adsorption of CO molecule (the latter being Lewis base) is widely considered as the measure of the Brønsted acidic strength in zeolites, and although it is not the only indicator, and even disputed by certain authors,[56] undoubtedly the scale of effect found in the dealuminated MAZ confirms its strong acidity. Interestingly, apart from the OH group with anomalously large redshift, the second band with a smaller redshift (280 cm^{-1}),[55] closer to the typical values reported in acidic zeolites (about 300 cm^{-1}) was also observed.[57] The main goal of the briefed work was the identification of distinct Brønsted sites in MAZ and explaining the differences between them.

In order to optimize structures of periodic models at the DFT level I employed again QUANTUM ESPRESSO package,[7] using PBE functional,[9] Vanderbilt ultrasoft pseudopotentials,[28] the cutoff energy of 400 eV and the Brillouin zone sampling limited to Γ point. As a model of dealuminated MAZ I used hexagonal cell doubled along the shortest lattice constant c, with one T site being occupied by Al atom, and with one O atom in AlO_4 unit being bound to H^+ ion, thus giving the supercell stoichiometry of $Si_{71}AlO_{144}H$. There are two inequivalent crystallographic T atoms positions and six O atoms positions, which gives – assuming that H^+ ion is always attached to O site within AlO_4 unit – seven different Brønsted acidic centers, namely T1O(1-4) and T2O(2,5,6), where TxOy denotes the crystallographic positions of Al atom and the protonated O one, respectively, see Fig. 15. The applied models agree with diffraction and spectroscopic studies on dealuminated MAZ, which showed that the crystal structure of MAZ is preserved after dealumination, and the vibrational frequencies of OH groups interacting with CO (3700 cm^{-1} <) stem from OH groups bridging T atoms and not from the silanol groups around the lattice defects formed upon the partial removal of Al atoms.[58] I estimated OH frequencies using semiempirical scaling methods, proposed by Nachtigall *et al.*, which allows obtaining anharmonic OH frequencies from the bond lengths and thus avoiding the computationally challenging phonon calculations for the large zeolite cell.[59] I considered CO binding to H^+ only via its carbon end (where the lone electron pair resides), as this type of adsorption is known to be energetically favorable in acidic zeolites.[57,59]

The stability order of optimized MAZ structures with various types of Brønsted sites is as follows: T2O5 > T1O3 = T2O2 ≈ T1O2 > T1O1 = T1O4 ≫ T2O6. The decrease in energy with respect to the most stable T2O5 sites is rather small (up to 10 kJ/mol) in all cases but the least stable T2O6 (destabilized by 30 kJ/mol). In the latter case, significantly lower stability can be associated with enforced structurally the large value of Al–O–Si angle(149°), clearly larger than the corresponding values for the remaining sites (129–136°). The strength of CO binding by acidic sites decreases in the order T1O1 ≈ T1O3 > T2O6 ≈ T1O4 > T1O2 ≈ T2O5 > T2O2. Roughly speaking, the ability to bind CO exhibits the opposite trend to the stability of OH groups, however, it is not exactly reciprocal. The optimal geometry of H···CO adducts is a nearly linear one and CO binding energy is lower therein, where the interaction with pore walls enforces a larger deviation (>10°) of H–C–O angle from 180° value. I assumed that the observed spectroscopically bands from CO adsorbing OH groups stem from these Brønsted sites, which are stable enough, to be appreciably populated in MAZ and yet interact strongly with CO molecules. Therefore, I excluded both the most stable T2O5 site, where CO adsorption breaks intralattice hydrogen bond OH···O, T2O2 one, where the proximity of pore wall prevents H···CO adduct

[56] E. G. Derouane, *et al. Cat. Rev. Sci. Eng.* **2013**, *55*, 454-515; C. O. Areán *et al.*, *Phys. Chem. Chem. Phys.* **2014** *16*, 10129-10141.

[57] C. O. Areaán, *J. Mol. Struct.* **2008**, *880*, 31-37.

[58] M. Gackowski *et al.*, *Appl. Catal. A* **2019**, *578*, 53-62.

[59] P. Nachtigall *et al.*, *Phys. Chem. Chem. Phys.* **2009**, *11*, 791-802.

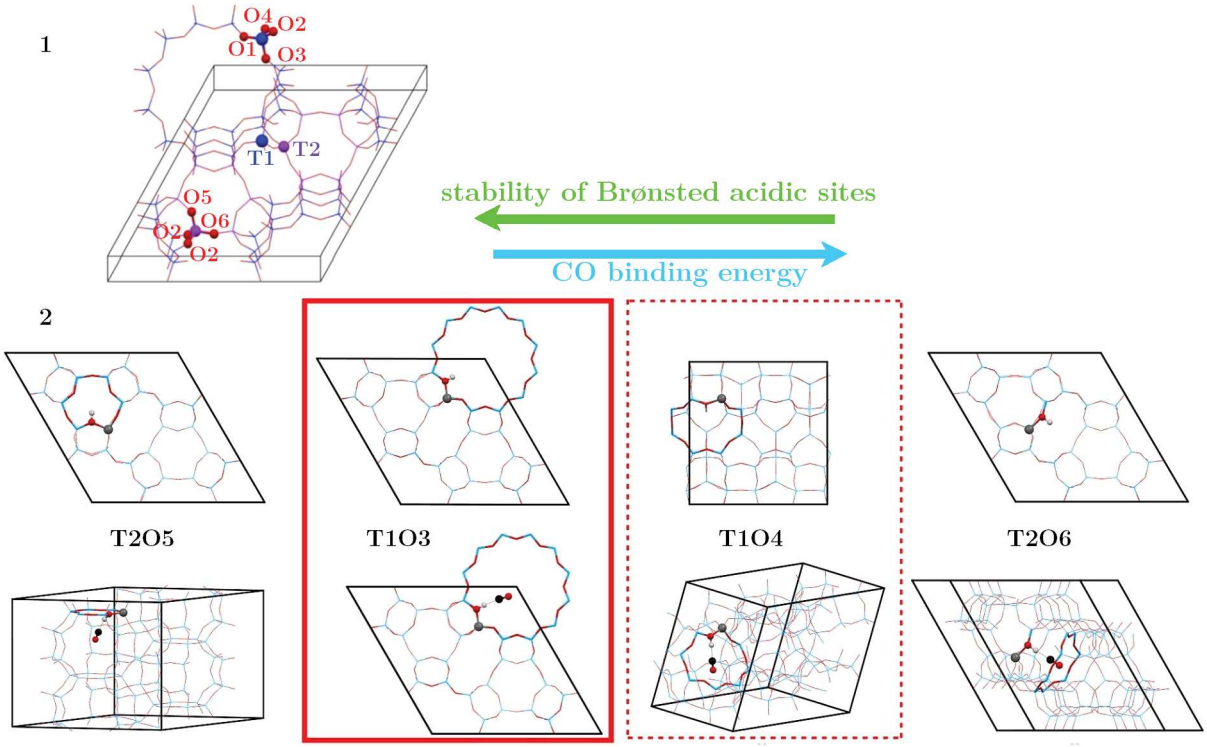

Figure 15: *CO adsorption on acid Brønsted sites in mazzite (MAZ) type zeolites: (1) Hexagonal MAZ unit cell with inequivalent crystallographic positions of T and O atoms depicted, the atoms in T1 and T2 positions depicted with blue and purple, respectively, O atoms colored in red. (2) The DFT/PBE optimized models of acid MAZ before and after CO adsorption. The bands with large and moderate redshift can be ascribed, respectively, to T1O3 site (CO adsorption within the main channel of MAZ) and T1O4 one (adsorption in smaller side cage). The elements coloring: C–black, O–red, Si–blue, Al–grey, H–white.*

from the adopting of linear structure, as well as T2O6, where CO binding is quite strong, but the stability of initial Brønsted site itself is low.

Eventually, I proposed the following assignment of OH bands: (i) the strongly redshifted band can be ascribed to T1O3 and T1O1 sites, wherein the adsorbed molecule points toward the main void of MAZ and the H···CO has a nearly linear structure (the computed redshift is about 360 cm^{-1}), (ii) the band with smaller redshift can be assigned to T1O4 sites, where CO molecule is located within the smaller cage and H···CO geometry is more bent (the computed redshift mounts to 315 cm^{-1}).

2.2.6 Summary

My scientific achievement is the cycle of papers devoted to the computational determination of structural, electronic, and spectroscopic properties of the various materials of practical importance, which chemistry is based on Si–O and/or Al–O connectivities: silicate [**H1**, **H2**, **H6**] and aluminate cements [**H3**, **H4**], ultramarine pigments [**H5**, **H8**], and catalytic zeolites [**H7**]. Owing to various computational approaches, (mainly the density functional theory level calculations, but also molecular mechanics and the correlated methods of quantum chemistry), I obtained many new results, being the important contribution to the state of knowledge of these materials, which clarified several discussed and insufficiently refined by experiment issues from the field of physics and chemistry of aluminosilicates, in some cases, I also proposed new experimental studies and their interpretation.

- Upon the first in literature simulations of ^{29}Si NMR spectra for the periodic models of C–S–H gel I showed that this main component of hydrated Portland cements structurally resembles rather 14Å tobermorite than jennite [**H1**].

- I demonstrated that the analysis of principal components of ^{29}Si chemical shift tensor in C–S–H enables unambiguous identification of silica tetrahedra of various condensation degree, even if they exhibit little difference in the isotropic chemical shift, which can be utilized in the future experimental studies on cements.[**H2**].

- I confirmed the instability of cubic ye'elimite structure with respect to orthorhombic or tetragonal distortion and proposed additional monoclinic polymorph of this mineral, not observed experimentally yet [**H3**].

- I explained the decrease in bulk modulus of Fe doped kaoite as the result of increased compressibility of Ca–O polyhedra, overwhelming the strengthening of hydrogen bond network [**H4**].

- In the first periodic and large cluster studies on blue ultramarines I showed that $S_3^{\bullet -}$ radicals occluded in the adjacent sodalite cages are not exchange coupled, their electronic and structural properties are only slightly affected by the interaction with the lattice, however, different local environments of $S_3^{\bullet -}$ radicals can affect the dynamics of these ions in confinement, resulting in observed EPR bands with different signal averaging [**H5**].

- Owing to periodic modeling of Ca_2SiO_4 I demonstrated that the less energetically stable and simultaneously more reactive with water polymorphs exhibit large departure from the octahedral Ca–O coordination and the softening of acoustic phonon modes, corresponding to the relative displacements of Ca^{2+} and SiO_4^{2-} ions [**H6**].

- In the first periodic DFT studies on mazzite type zeolites, I assigned two observed experimentally upon CO adsorption infrared bands of OH groups to Brønsted acidic sites located in cavities of different sizes [**H7**].

- Owing to the first periodic and cluster DFT modeling of red ultramarines I confirmed the assignment of the red chromophore in ultramarines to the planar isomer of S_4 molecule of C_{2v} symmetry, I showed S_4 and $S_4^{\bullet -}$ in condensed phase, as well as predicted the characteristic features of UV-Vis-NIR and EPR spectra of $S_4^{\bullet -}$ ions, the latter results should facilitate the experimental detection of these radicals [**H8**].

3 Presentation of significant scientific activities realized in more than one scientific institution

In the years 2010–2013, I hold a postdoctoral position at Donostia International Physics Center, where, within the group of prof. Andrés Ayuela, I conducted computational studies on structural and spectroscopic properties of cements. This collaboration lasts to the present day, and I have included five common papers into the current scientific achievement.

In my current workplace, Institute of Physics PAS I support with atomistic simulations the experimental studies, performed in the SL 1.2 group, on metal complexes of biological importance. These studies are undertaken in collaboration with prof. Marta Struga from Dept. of Medicine, Medical University of Warsaw (new pharmacological compounds), and prof. Wiesława Ferenc Dept. of Chemistry, Maria Curie—Skłodowska University (metal complexation with herbicides). For one of the papers, resulting from these studies, I obtained together with my colleagues the third degree group award from the rector of Warsaw Medical University.

As a part of my employment in the EAgLE project I visited in 2015 ALBA synchrotron, where I was one of two persons conducting classes within „Wien2k & Turbomole Workshop": I delivered 4 lectures and co-conducted 10 hours of practical exercises on molecular modeling. The effect of this visit was the extension of collaboration with prof. Miguel Aranda (the first common project we had during my postdoctoral internship) and the new collaboration with prof. Eric Pellegrin. The aforementioned cooperation resulted in two published papers, of which I included one in the scientific achievement.

The collaboration with prof. Ewa Brocławik (my PhD supervisor) and prof. Jerzy Datka from Jerzy Haber Institute of Catalysis and Surface Chemistry PAS, resulted in three papers (two original research articles and one review), one of these papers is included in the scientific achievement. Moreover, I presented the latter results at conferences organized by the Institute of Catalysis and Surface Chemistry PAS (2018 and 2019), in 2017 I delivered a talk on the institute seminar.

4 Presentation of didactic, science popularization and event organization activities

Didactic activity

1. 08.-09.**2015** Co-tutor of summer student internship at Institute of Physics PAS, SL-1.2 group. The subject: "The characterization of bioactive organic and metal–organic materials with spectroscopic techniques and molecular modeling".

2. 16-20.11.**2015** The lecturer and conducting excercises during *"Wien2k & Turbomole Workshop"*, ALBA synchrotron, Barcelona.
   Lectures: (i) "Exploring Potential Energy Surface", (ii) "Hartree-Fock method and beyond", (iii) "Chemically biased introduction to Density Functional Theory", (iv) "Introduction to Turbomole package"; 10 lesson hours of hands-on computer exercises with Turbomole program.

3. 07.**2016** Co-tutor of summer student internship at Institute of Physics PAS, SL-1.2 group. The subject: "XPS, UV-Vis and FTIR spectra of complexes of 4—bromophenoxyacetic acid win nickel".

4. 01.**2019** Co-tutor in the workshop for the high school talented youth at Institute of Physics PAS, SL-1.2 group. The subject: "Synthesis of bioactive metal complexes and their characterization with IR spectroscop".

Event organization

Event co-organizer: *"Workshop on Molecular Simulation and Drug Design"*, 08-11.09.**2015**, Institute of Physics PAS (within EAgLE project).

5 Other scientific activities and accomplishments

Papers published before PhD title

[D1] E. Broclawik, **P. Rejmak**, P. Kozyra, J. Datka, "DFT quantum chemical modeling of the interaction of alkenes with Cu^+ sites in zeolites", *Catalysis Today* **2006**, *114*, 162–168,
IF_{2021} = 6.562, citations = 13.

[D2] **P. Rejmak**, M. Sierka, J. Sauer, "Theoretical studies of Cu(I) sites in faujasite and their interaction with carbon monoxide", *Physical Chemistry Chemical Physics* **2007**, *9*, 5446–5456,
IF_{2021} = 3.945, citations = 36.

[D3] E. Banach, P. Kozyra, **P. Rejmak**, E. Broclawik, J. Datka, "Cobalt cationic sites in ferrierites: QM/MM modeling", *Catalysis Today* **2008**, *137*, 493–497,
IF_{2021} = 6.562, citations = 7.

[D4] **P. Rejmak**, E. Broclawik, K. Gora-Marek, M. Radon, J. Datka, "Nitrogen Monoxide Interaction with Cu(I) Sites in Zeolites X and Y: Quantum Chemical Calculations and IR Studies", *Journal of Physical Chemistry C* **2008**, *112*, 17998–18010,
IF_{2021} = 4.177, citations = 28.

Papers published after PhD title, not included in the discussed scientific achievement

[P1] **P. Rejmak**, M. Mitoraj, E. Broclawik, "Electronic view on ethene adsorption in Cu(I) exchanged zeolites", *Physical Chemistry Chemical Physics* **2010**, *12*, 2321–2330.
IF_{2021} = 3.945, citations = 17, corresponding author.

[P2] M. T. Klepka, A. Drzewiecka-Antonik, A. Wolska, **P. Rejmak**, K. Ostrowska, E. Hejchman, H. Kruszewska, A. Czajkowska, I. Mlynarczuk Bialy, W. Ferenc, "Synthesis, structural studies and biological activity of new Cu(II) complexes with acetyl derivatives of 7-hydroxy-4-methylcoumarin", *Journal of Inorganic Biochemistry* **2015**, *145*, 94–100.
IF_{2021} = 4.336, citations = 20.

[P3] M. Radon, **P. Rejmak**, M. Fitta, M. Balanda, J. Szklarzewicz, "How can $[Mo^{IV}(CN)_6]^{2-}$, an apparently octahedral $(d)^2$ complex, be diamagnetic? Insights from quantum chemical calculations and magnetic susceptibility measurements", *Physical Chemistry Chemical Physics* **2015**, *17*, 14890–14902.
IF_{2021} = 3.945, citations = 8.

[P4] A. Drzewiecka-Antonik, W. Ferenc, A. Wolska, M. T. Klepka, B. Cristovao, J. Sarzynski, **P. Rejmak**, D. Osypiuk, "The Co(II), Ni(II) and Cu(II) complexes with herbicide 2,4-dichlorophenoxyacetic acid - Synthesis and structural studies", *Chemical Physics Letters* **2017**, *667*, 192–198.
IF_{2021} = 2.719, citations = 18.

[P5] M. T. Klepka, A. Wolska, A. Drzewiecka-Antonik, **P. Rejmak**, K. Hatada, G. Aquilanti, "XAFS study of bioactive Cu(II) complexes of 7-hydroxycoumarin derivatives in organic solvents", *Chemical Physics Letters* **2017**, *673*, 113–117.
IF_{2021} = 2.719, citations = 1.

[P6] A. Drzewiecka-Antonik, A. E. Koziol, **P. Rejmak**, K. Lawniczak-Jablonska, L. Nittler, T. Lis, "Novel Ba(II) and Pb(II) coordination polymers based on citric acid: Synthesis, crystal structure and DFT studies", *Polyhedron* **2017**, *132*, 1–11.
IF_{2021} = 2.975, citations = 8.

[P7] A. Drzewiecka-Antonik, W. Ferenc, **P. Rejmak**, A. Wolska, M. T. Klepka, B. Cristovao, B. Miroslaw, J. Sarzynski, D. Osypiuk, "Coordination environment of new Co(II), Ni(II) and Cu(II) complexes with 4-bromophenoxyacetic acid: Structural, spectroscopic and theoretical studies", *Polyhedron* **2017**, *133*, 54–62.
IF_{2021} = 2.975, citations = 7.

[P8] A. Drzewiecka-Antonik, **P. Rejmak**, M. T. Klepka, A. Wolska, P. Pietrzyk, K. Stępień, G. Sanna, M. Struga, "Synthesis, structural studies and biological activity of novel Cu(II) complexes with thiourea derivatives of 4-azatricyclo[5.2.1.0(2,6)] dec-8-ene-3, 5-dione", *Journal of Inorganic Biochemistry* **2017**, *176*, 8–16.
IF_{2021} = 4.336, citations = 15.

[P9] M. T. Klepka, A. Drzewiecka-Antonik, A. Wolska, **P. Rejmak**, M. Struga, "Structural studies of Cu(II) complexes with coumarin acid derivatives obtained using direct and electrochemical synthesis", *Chemical Physics Letters* **2018**, *691*, 190–195.
IF_{2021} = 2.719, citations = 5.

[P10] A. Bielenica, A. Drzewiecka-Antonik, **P. Rejmak**, J. Stefanska, M. Kolinski, S. Kmiecik, B. Lesyng, M. Wlodarczyk, P. Pietrzyk, M. Struga, "Synthesis, structural and antimicrobial studies of type II topoisomerase-targeted copper(II) complexes of 1,3-disubstituted thiourea ligands", *Journal of Inorganic Biochemistry* **2018**, *182*, 61–70.
IF_{2021} = 4.336, citations = 14.

[P11] **P. Rejmak**, J. Datka, E. Broclawik, "Fine speciation of active sites in zeolites by a CO probe: Dynamics and IR frequencies", *International Journal of Quantum Chemistry* **2018**, *118*, e25873.
IF_{2021} = 2.437, citations = 6.

[P12] K. Lawniczak-Jablonska, A. Wolska, P. Kuzmiuk, **P. Rejmak**, K. Kosiel, "Local atomic order of the amorphous TaOx thin films in relation to their chemical resistivity", *RSC Advances* **2019**, *9*, 35727–35734.
IF_{2021} = 4.036, citations = 4.

[P13] E. Pellegrin, V. Perez-Dieste, C. Escudero, **P. Rejmak**, N. Gonzalez, A. Fontsere, J. Prat, J. Fraxedas, S. Ferrer, "Water/methanol solutions characterized by liquid μ-jet XPS and DFT–The methanol hydration case", *Journal of Molecular Liquids* **2020**, *300*, 112258.
IF_{2021} = 6.633, citations = 4.

[P14] A. Drzewiecka-Antonik, **P. Rejmak**, M. Klepka, A. Wolska, A. Chrzanowska, M. Struga, "Structure and anticancer activity of Cu(II) complexes with (bromophenyl)thiourea moiety attached to the polycyclic imide", *Journal of Inorganic Biochemistry* **2020**, *212*, 111234.
IF_{2021} = 4.336, citations = 7.

[P15] E. Broclawik, P. Kozyra, M. Mitoraj, M. Radoń, **P. Rejmak**, "Zeolites at the Molecular Level: What Can Be Learned from Molecular Modeling", *Molecules* **2021**, *26*, 1511.
IF_{2021} = 4.927, citations = 1, artykuł przeglądowy.

Book chapter

E. Broclawik, M. Mitoraj, **P. Rejmak**, A. Michalak, "From electron density flow towards activation: Metal sites in zeolites from the combined Extended Transition State (ETS) Method and the Natural Orbitals for Chemical Valence (NOCV) perspective" in *Handbook of Inorganic Chemistry Research*, (Ed.: D. Morrison), Chemistry Research and Applications, **2010**, pp. 361–383.
Citations = 3.

Reviewing activity in scientific journals

1. *Nature Communications* **2015**
2. *Journal of Physical Chemistry C* **2016**
3. *Construction and Building Materials* **2019**
4. *Solid State Communications* **2020**
5. *Applied Surface Science* **2020**

Seminars and lectures

[S1] "QM/MM studies on Cu(I) sites in zeolites and their interactions with small molecules", Donostia International Physics Center seminar, Donostia-San Sebastián, 25.03.**2010**.

[S2] "Theoretical ^{29}Si NMR in hydrated Portland cement", *2nd nanoIKER Workshop*, Bizkaia Science and Technology Park, Derio, 10.06.**2013**.

[S3] "Modelowanie centrów Cu(I) w zeolitach i ich oddziaływań z małymi cząsteczkami metodami QM/MM", Roentgen group seminar, Institute of Physics PAS, Warszawa, 14.01.**2014**.

[S4] "Exploration of Potential Energy Surface", Roentgen group seminar, Institute of Physics PAS, Warszawa, 25.03.**2014**.

[S5] "Hartree-Fock Method and Boldly Beyond", Roentgen group seminar, Institute of Physics PAS, Warszawa, 15.04.**2014**.

[S6] "Crash Course in The Density Functional Theory", Roentgen group seminar, Institute of Physics PAS, Warszawa, 13.05.**2014**.

[S7] "Basics of UV-Vis Absorption Spectroscopy", Roentgen group seminar, Institute of Physics PAS, Warszawa, 16.03.**2015**.

[S8] "Modelowanie katalitycznych centrów Cu(I) w zeolitach metodami QM/MM", Division of Condensed Matter Physics seminar, Henryk Niewodniczańskiego Institute of Nuclear Physics, Kraków, 15.02.**2016**.

[S9] "Badania strukturalne bioaktywnych komleksów Cu(II) metodami obliczeniowymi i absorpcyjnej spektroskopii rentgenowskiej", Jerzy Haber Institute of Catalysis and Surface Chemistry PAS seminar, Kraków, 29.11.**2017**.

[S10] "Computational studies on blue and red ultramarines", Theoretical Chemistry Department seminar, Faculty of Chemistry, Jagiellonian University, Kraków, 26.01.**2022**.

Oral communications at conferences

[O1] **P. Rejmak**, J. S. Dolado, M. J. Stott, A. Ayuela, "^{29}Si NMR spectroscopy on cements: A theoretical study on CSH gel", *1st Baskrete Open Days*, Donostia-San Sebastián, 13-14.03.**2012**.

[O2] **P. Rejmak**, J. S. Dolado, M. J. Stott, A. Ayuela, "Computational study on ^{29}Si NMR in hydrated Portland cement ", *VIIth Symposium on Nuclear Magnetic Resonance in Chemistry, Physics and Biological Sciences*, Warszawa, 26-28.09.**2012**.

[O3] **P. Rejmak**, J. S. Dolado, M. J. Stott, A. Ayuela, "^{29}Si chemical shifts anisotopies in hydrated calcium silicates: A computational study", *2nd Baskrete Open Days*, Donostia-San Sebastián, 28-29.05.**2013**.

[O4] **P. Rejmak**, J. S. Dolado, M. J. Stott, A. Ayuela, "Computational ^{29}Si NMR in hydrated Portland cement", *Current Trends in Theoretical Chemistry VI*, Kraków, 01-05.09.**2013**.

[O5] **P. Rejmak**, J. S. Dolado, M. J. Stott, A. Ayuela, "Symulowanie widm ^{29}Si NMR dla cementu portlandzkiego", *VII Ogólnopolskie Sympozjum "Nauka i Przemysł"*, Lublin, 10-12.06.**2014**.

[O6] **P. Rejmak**, A. Drzewiecka-Antonik, M. Klepka, A. Wolska, P. Pietrzyk, M. Struga, "Determining the structure of novel bioactive Cu(II)-thiourea complexes by combined XAFS spectroscopy, laboratory techniques and DFT calculations", *XII Krajowe Sympozjum Użytkowników Promieniowania Synchrotronowego KSUPS'17*, Gdańsk, 04-07.09.
2017.

[O7] **P. Rejmak**, A. Drzewiecka-Antonik, M. Klepka, A. Wolska, P. Pietrzyk, M. Struga, "Refining the structures of novel Cu(II) bioactive complexes: XAFS spectroscopy, laboratory techniques and DFT calculations", *17th International Conference on X-ray Absorption Fine Structure*, Kraków, 22-27.07.**2018**.

[O8] **P. Rejmak**, M. Gackowski, Ł. Kuterasiński, J. Podobiński, B. Sulikowski, J. Datka, E. Brocławik, "Physicochemical and catalytic properties of active sites in hierarchical mazzite revealed by IR and NMR spectroscopies combined with DFT modeling", *51 Ogólnopolskie Kolokwium Katalityczne*, Kraków, 13-14.03.**2019**.

[O9] **P. Rejmak**, "Rozwiązanie zagadki czerwonego chromoforu w pigmentach typu ultramaryn metodami obliczeniowymi", *IV Ogólnopolskie Forum Chemii Nieorganicznej*, Toruń, 07-09.09.**2021**.

Other achievements

Over 15 posters presented at domestic and international conferences.

The third degree group award of the rector of the Medical University of Warsaw for the paper published in *J. Inorg. Biochem* **2017**, *176*, 8.